The steady-state response of a rotating ring subjected to a stationary load

Lu, Tao; Tsouvalas, Apostolos; Metrikine, Andrei

DOI
10.1016/j.ijsolstr.2020.06.011

Publication date
2020

Document Version
Final published version

Published in
International Journal of Solids and Structures

International Journal of Solids and Structures 202 (2020) 319–337

Contents lists available at ScienceDirect

International Journal of Solids and Structures

journal homepage: www.elsevier.com/locate/ijsolstr

The steady-state response of a rotating ring subjected to a stationary load

T. Lu *, A. Tsouvalas, A.V. Metrikine

Faculty of Civil Engineering and Geosciences, Delft University of Technology, Stevinweg 1, 2628 CN Delft, The Netherlands

ARTICLE INFO

Article history:
Received 23 October 2019
Received in revised form 7 June 2020
Accepted 9 June 2020
Available online 20 June 2020

Keywords:
Rotating ring on elastic foundation
Plane strain
High-order model
In-plane vibrations
Steady-state response
Method of the images
Resonance speeds

ABSTRACT

The in-plane steady-state response of a rotating ring on elastic foundation subjected to a stationary load is investigated theoretically using a high-order model in the framework of the plane strain assumption. The adopted high-order model accounts for the through-thickness variation of stresses and displacements, as well as the boundary tractions at the inner and outer surfaces of the ring. Based on the ratio of the foundation stiffness to the stiffness of the ring, two configurations of the ring-on-foundation system are investigated, namely soft foundation (stiff ring) and stiff foundation (soft ring). The analytical "method of the images" is used to obtain the ring response. It is found that the response of a stiff ring to a stationary load of constant magnitude is governed by the translational rigid body-like motion. In contrast, in the case of a soft ring, a wave-like deformation is predicted for the rotational speeds higher than a critical one. It is for the first time that such wave-like displacements are predicted using a rotating ring model with the rotation effects being properly considered. The response of a rotating ring to a stationary harmonic load is studied too. The predicted displacements using the high-order model are compared with those obtained from the classical low-order model in which only the radial and circumferential displacements at the middle surface of the ring are considered. It is concluded that only in the case of a stiff ring, the classical low-order model and the high-order model give similar predictions. When the ring is soft, the predictions of the two models deviate significantly. Resonances of a stationary ring under a moving load and a rotating ring subjected to a stationary load are compared in terms of the resonance speeds and the steady-state responses. It is shown that these two situations can not be treated as equal in many cases.

1. Introduction

Rotating ring-like structures are very commonly used in civil, mechanical and aerospace engineering. Typical examples of such structures are components in turbomachinery (Macke, 1966), compliant gears (Cooley and Parker, 2014), flexible train wheels (Noga et al., 2014), conventional pneumatic tyres (Gong, 1989) and more recent non-pneumatic tyres (Gasmi et al., 2012). At the micro-scale, rotating ring models find their applications in the field of ring gyroscopes (Yoon et al., 2015), in which high accuracy of modelling is required. The in-plane vibrations of rotating rings are of particular interest since the above-mentioned structures are usually subjected to in-plane loads.

The main points of attention in the studies on the dynamic response of the rotating rings are the existence and severity of resonances and the occurrence of the so-called "standing waves" which is a stationary deformation pattern observed in rolling pneumatic tires (Padovan, 1976; Chatterjee et al., 1999). Despite the absence of consensus on the existence of resonances of a rotating ring subjected to a stationary load with constant magnitude (Endo et al., 1984; Huang and Soedel, 1987; Lin and Soedel, 1988; Krylov and Gilbert, 2010; Graham, 2013; Krylov, 2013; Lu and Metrikine, 2015), a seemingly conclusive result has been obtained in Lu et al. (2019) according to which resonance can occur in rotating rings. Modes which are stationary as observed in a space-fixed reference system, are excited by the load (Soedel, 2004) when a ring rotates at high speeds, resulting in a steady-state response which is time-invariant to a space-fixed observer. The experimental evidence of such a response is the occurrence of the stationary deformation patterns in rolling tires (Chatterjee et al., 1999; Cho et al., 2007). Similar wave phenomena have been reported in soft calenders of paper machines (Karttunen, 2015).

Apart from the numerical modelling e.g. in Padovan (1975), Kennedy and Padovan (1987), Cho et al. (2007), Karttunen and von Hertzen (2013), efforts into theoretical prediction of the wave-like steady-state response can be found in Padovan (1976), Potts et al. (1977), Soedel (1975), Chatterjee et al. (1999), Karttunen and von Hertzen (2016), Krylov and Gilbert (2010). However, in these models either the bending stiffness is not considered (Chatterjee

* Corresponding author.
E-mail address: T.Lu-2@tudelft.nl (T. Lu).

https://doi.org/10.1016/j.ijsolstr.2020.06.011
0020-7683/

et al., 1999; Karttunen and von Hertzen, 2016) or the rotation effects are not properly accounted for Padovan (1976), Potts et al. (1977), Soedel (1975), Krylov and Gilbert (2010). For example, the rotation-induced hoop tension is not considered in Padovan (1976), Potts et al. (1977) and in Soedel (1975), Krylov and Gilbert (2010) all the rotation effects are neglected. The rotation effects, namely the centrifugal force that leads to an axisymmetric radial expansion and a hoop stress, and the Coriolis force are essential to determine the dynamic behaviour of rotating rings (Lu et al., 2019; Lu, 2019). The stationary wavy deformation has not been successfully predicted so far using a *rotating ring model* which properly considers the rotation effects.

In this paper, the high-order model is adopted from Lu et al. (2019) to simulate the in-plane response of rotating rings on elastic foundation to a stationary load. The primary aim is to investigate the ring response at resonance speeds and to analyze the steady-state deflection patterns of the ring rotating at speeds lower and higher than the minimum resonance speed. The steady-state response of a rotating ring subjected to a constant stationary load is calculated using the "method of the images" (Metrikine and Tochilin, 2000). The responses are computed for the cases of soft foundation (stiff ring) and stiff foundation (soft ring). The influences of the relative value of the foundation stiffness and the ring stiffness are therefore thoroughly addressed. Applying a stationary constant load, results show that the $n = 1$ mode governs the response of the soft foundation (stiff ring) case, leading to a translational rigid body-like motion of the ring. On the contrary, a localised response occurs for a soft ring that rotates sub-critically, i.e. at speeds lower than the minimum resonance speed, whereas a wave-like deformation pattern is predicted when the ring rotates super-critically. The differences in predicted displacements between the classical model and the high-order model are investigated. The applicability and limitations of the classical model in predicting the dynamic response of rotating rings are addressed.

Besides the case of rotating rings under stationary load, it is also common in engineering practice that a stationary ring is subjected to a circumferentially moving load. Investigations of the steady-state responses in such a case can be found in Metrikine and Tochilin (2000), Forbes and Randall (2008), Karttunen and von Hertzen (2014), Karttunen and von Hertzen (2016). It is concluded (Karttunen and von Hertzen, 2014) that the effect of rotation is negligible and the rotating ring under stationary load and stationary ring under moving load can be treated as equal. In this paper, the two cases are compared with the focus placed on the steady-state responses and, particularly, the resonance speeds. It is shown that these two cases need to be distinguished.

The main original contribution of this paper lies in the theoretical prediction of a wave-like stationary deformation pattern which occurs in a rotating ring subjected to a stationary load. A proper consideration of the rotation effects is the key that makes it possible to distinguish the range of parameters in which the wave-like pattern can occur. This has not been done in the past. In general, the results obtained in this paper close the debate on the existence of resonances of rotating rings under a stationary load and demonstrate the applicability and limitations of the classical rotating thin ring models in predicting the forced vibrations.

The paper is structured as follows. Section 2 gives the complete description of the mathematical statement of the problem and the procedure to solve it. Subsequently, the steady-state responses of rotating rings under stationary constant and harmonic loads are discussed in Section 3 and the influence of the foundation stiffness on the dynamic response is thoroughly investigated. In Section 4, resonance speeds, as well as the dynamic responses, are discussed for the stationary ring under moving load and the rotating ring subjected to stationary load cases. Finally, Section 5 summarises the main conclusions of this paper.

2. Model and the "method of the images

A rotating ring on elastic foundation subjected to a stationary load is shown in Fig. 1. The inner surface of the ring is connected to an immovable axis by distributed radial and circumferential springs (the foundation). The ring rotates at a constant angular speed Ω. A space-fixed coordinate system (r, θ) is adopted to describe the motions of the ring. It is assumed that the mean radius of the ring is R. To simplify mathematical expressions, an auxiliary coordinate z is introduced as $z = r - R$, in which r defines the radial coordinate, i.e. the ring occupies the space $R - h/2 \leqslant r \leqslant R + h/2$ where h is the thickness of the ring. The in-plane radial and circumferential displacements of the ring with respect to the undeformed configuration are designated by $w(z, \theta, t)$ and $u(z, \theta, t)$, respectively. The stiffnesses of the radial and circumferential springs per unit area are designated as k_r and k_c, respectively. Furthermore, ρ is the mass density of the ring, E is the Young's modulus, G is the shear modulus, v is the Poisson's ratio, λ and μ are the Lamé constants. In addition to R and h, the geometrical parameters are: A is the cross-sectional area, I is the cross-sectional moment of inertia, b is the width of the ring.

The high-order model of the ring developed in Lu et al. (2019) is employed. Plane strain configuration is assumed for the model. The external load is incorporated in the governing equations by the Hamilton's principle. The technique of solving the governing equations is demonstrated in this section as well.

2.1. Complete description of the problem

To include external loading in the governing equations by the Hamilton's principle, the work done by the external loads needs to be formulated. Considering a radial load $F(\theta, z, t)$ that is uniformly distributed over the ring width as shown in Fig. 1, the variation of the work done by this load reads

$$\begin{aligned}\int_{t_1}^{t_2} \delta W \,\mathrm{d}t &= b \int_{t_1}^{t_2} \int_{-h/2}^{h/2} \int_0^{2\pi} \delta W_{\text{in}} r \,\mathrm{d}\theta \mathrm{d}z \mathrm{d}t \\ &= b \int_{t_1}^{t_2} \int_{-h/2}^{h/2} \int_0^{2\pi} F(\theta, z, t)\, \delta w\, r \,\mathrm{d}\theta \mathrm{d}z \mathrm{d}t. \end{aligned} \tag{1}$$

The load is applied along the width on the outer ring surface and thus is given as $F(\theta, z, t) = P(\theta, t)\delta(z - h/2)$ in which δ is the Dirac function. Note that θ is the polar coordinate of the non-rotating coordinate system. It is assumed that the ring experiences a uniform radial expansion due to steady rotation before the load is applied. The radial displacement w is defined as positive when it points outward and the positive direction of the circumferential displacement u is defined as counter-clockwise. Then Eq. (1) becomes

$$b \int_{t_1}^{t_2} \int_{-h/2}^{h/2} \int_0^{2\pi} \delta W_{\text{in}} r \,\mathrm{d}\theta \mathrm{d}z \mathrm{d}t = b \int_{t_1}^{t_2} \int_{-h/2}^{h/2} \int_0^{2\pi} \Big(P(\theta, t) \underset{\text{Dirac function}}{\downarrow} \delta(z - \frac{h}{2}) \Big) \underset{\text{variation}}{\uparrow} \delta w \, r \,\mathrm{d}\theta \mathrm{d}z \mathrm{d}t \tag{2}$$

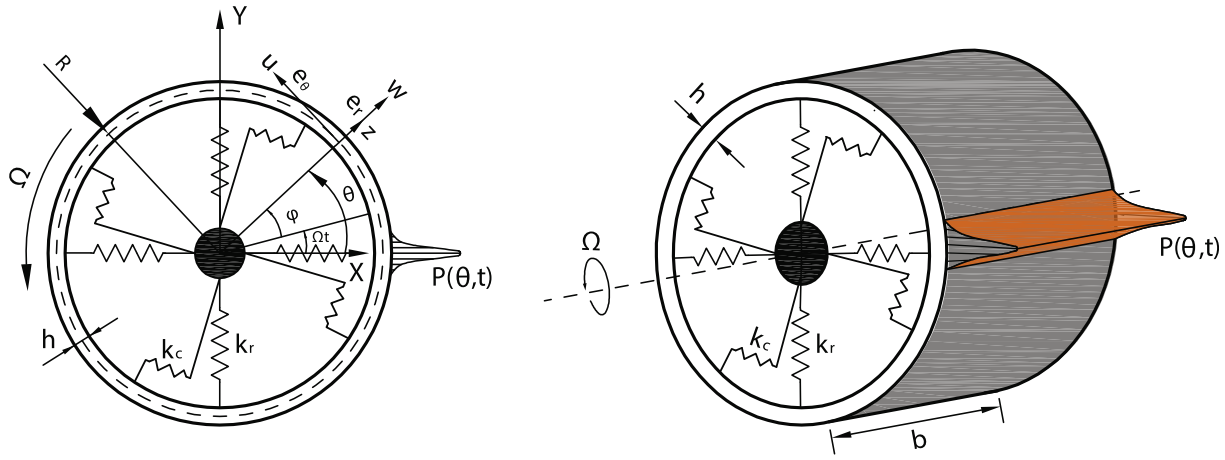

Fig. 1. A rotating ring on elastic foundation subjected to a stationary load: left figure for front view; right figure for side view.

The high-order model is adopted from Lu et al. (2019). For the expressions of the kinetic and potential energies and detailed derivation of the governing equations one is referred to Appendix A and Lu et al. (2019). According to Lu et al. (2019), the displacement fields are expressed as polynomial functions of the thickness z:

$$w(z,\theta,t)=\sum_{l=0}^{l=N_1} w_l(\theta,t)z^l,\quad u(z,\theta,t)=\sum_{q=0}^{q=N_2} u_q(\theta,t)z^q \tag{3}$$

in which l,q are integers and $l\geqslant 0, q\geqslant 0$. N_1 and N_2 are the orders of the polynomials of the displacement fields. Therefore, the variation of the radial displacement at the outer surface of the ring, namely $\delta\left(w|_{z=h/2}\right)$ in Eq. (2) is given by

$$\delta\left(w|_{z=h/2}\right)=\sum_{l=0}^{l=N_1}\delta w_l (h/2)^l. \tag{4}$$

The derivation of the homogeneous governing equations of the high-order model can be found in Lu et al. (2019). Adding the external loading terms at the right-hand side of the homogeneous governing equations, the equations of motion that govern the small vibrations about the static equilibrium in the radial direction are:

$$\begin{aligned}&\int_{\frac{-h}{2}}^{\frac{h}{2}}\left(\mathrm{I}_1^{\mathrm{lin}}z^l\right)\mathrm{d}z+\rho\int_{\frac{-h}{2}}^{\frac{h}{2}}\left(r\left(\dot{v}_1+\Omega v_1'-\Omega v_2\right)z^l\right)\mathrm{d}z\\&\quad+\left(f_1^{\mathrm{lin}}-f_2^{\mathrm{lin}}(-1)^l\right)\left(\tfrac{h}{2}\right)^l\\&\quad=-\left(\tfrac{h}{2}\right)^l P(\theta,t)(R+h/2),\ \ (l=0,1,2,3\ldots N_1).\end{aligned} \tag{5}$$

The linearised equations of motion in the circumferential direction are (Lu et al., 2019):

$$\begin{aligned}&\int_{\frac{-h}{2}}^{\frac{h}{2}}\left(\mathrm{I}_2^{\mathrm{lin}}z^q\right)\mathrm{d}z+\rho\int_{\frac{-h}{2}}^{\frac{h}{2}}\left(r\left(\dot{v}_2+\Omega v_{2\prime}+\Omega v_1\right)z^q\right)\mathrm{d}z\\&\quad+\left(f_3^{\mathrm{lin}}-f_4^{\mathrm{lin}}(-1)^q\right)\left(\tfrac{h}{2}\right)^q=0,\ (q=0,1,2,3\ldots N_2).\end{aligned} \tag{6}$$

The details of the expressions for $\mathrm{I}_1^{\mathrm{lin}},\mathrm{I}_2^{\mathrm{lin}},f_1^{\mathrm{lin}}$ through f_4^{lin} and the velocities v_1 and v_2 of a differential element of the ring in radial and circumferential directions in the left-hand side of Eqs. 5,6 can be found in Appendix B as well as in Lu et al. (2019). The coupling caused by rotation is similar to the classical low-order theory for rotating thin rings (Cooley and Parker, 2014) regarding the contributions of rotation to the gyroscopic, stiffness and centripetal operators. Due to the closeness of the ring, the load applies periodically with a spatial period of 2π. The dynamic responses need to comply with the periodicity condition, i.e.:

$$\begin{aligned}w_{\mathrm{d}}(z,0,t)&=\sum_{l=0}^{l=N_1}w_{\mathrm{ld}}(0,t)z^l=w_{\mathrm{d}}(z,2\pi,t)=\sum_{l=0}^{l=N_1}w_{\mathrm{ld}}(2\pi,t)z^l,\\u_{\mathrm{d}}(z,0,t)&=\sum_{q=0}^{q=N_2}u_{\mathrm{qd}}(0,t)z^q=u_{\mathrm{d}}(z,2\pi,t)=\sum_{q=0}^{q=N_2}u_{\mathrm{qd}}(2\pi,t)z^q.\end{aligned} \tag{7}$$

Eq. (7) can be rewritten as

$$\begin{aligned}w_{\mathrm{d}}(z,0,t)-w_{\mathrm{d}}(z,2\pi,t)&=\sum_{l=0}^{l=N_1}w_{\mathrm{ld}}(0,t)z^l-\sum_{l=0}^{l=N_1}w_{\mathrm{ld}}(2\pi,t)z^l\\&=\sum_{l=0}^{l=N_1}[w_{\mathrm{ld}}(0,t)-w_{\mathrm{ld}}(2\pi,t)]z^l=0\end{aligned} \tag{8}$$

and

$$\begin{aligned}u_{\mathrm{d}}(z,0,t)-u_{\mathrm{d}}(z,2\pi,t)&=\sum_{q=0}^{q=N_2}u_{\mathrm{qd}}(0,t)z^q-\sum_{q=0}^{q=N_2}u_{\mathrm{qd}}(2\pi,t)z^q\\&=\sum_{q=0}^{q=N_2}\left[u_{\mathrm{qd}}(0,t)-u_{\mathrm{qd}}(2\pi,t)\right]z^q=0\end{aligned} \tag{9}$$

For Eqs. 8 and 9 to be valid for all values of z, each component of the displacement expansion should satisfy the same periodicity condition:

$$w_{\mathrm{ld}}(0,t)=w_{\mathrm{ld}}(2\pi,t),\ \ u_{\mathrm{qd}}(0,t)=u_{\mathrm{qd}}(2\pi,t). \tag{10}$$

The subscript 'd' in Eqs. (7)–(10) stands for the dynamic displacements and is hereafter omitted for the sake of brevity. Eqs. (5)–(10) complete the description of a rotating ring subjected to a stationary load under plane strain assumption.

The solutions will be sought for in dimensionless form. The following dimensionless parameters are introduced (Graff, 1975):

$$\begin{aligned}&k=\sqrt{EI/(EA)},\quad \bar{k}=k/R,\quad \bar{\gamma}=n\bar{k},\quad \bar{\omega}=\omega k/c_0,\quad \bar{v}=R\Omega/c_0,\\&(\bar{k}_r,\bar{k}_c)=(k_r,k_c)k^2/(Eh),\quad W_{0\mathrm{e}}=w_{0\mathrm{e}}/R,\quad \bar{\theta}=\theta/\bar{k},\quad \tau=c_0t/k,\end{aligned} \tag{11}$$

where $c_0=\sqrt{E/\rho}$ is the speed of the longitudinal wave in the rod, $I=bh^3/12$ is the cross section area moment of inertia and $\bar{k}$ is the non-dimensional radius of gyration. $\bar{\theta}$ and τ are the dimensionless angle and temporal variables, respectively. Introducing a dimensionless

coordinate $\bar{z}=z/h$ in the radial direction, the dimensionless displacements are defined as

$$W(\bar{z},\bar{\theta},\tau)=w(z,\theta,t)/R,\ U(\bar{z},\bar{\theta},\tau)=u(z,\theta,t)/R \tag{12}$$

and therefore

$$W_l(\bar{\theta},\tau)=h^l w_l(\theta,t)/R,\ U_q(\bar{\theta},\tau)=h^q u_q(\theta,t)/R,\quad (l=0,1,2,3\ldots N_1, q=0,1,2,3\ldots N_2). \tag{13}$$

in the dimensionless coordinate system $\{\bar{z},\bar{\theta},\tau\}$.

2.2. The classical low-order model

The equations that govern vibrations of a rotating ring subjected to a stationary load from the classical theory in space-fixed coordinate are (Cooley and Parker, 2014):

$$\begin{aligned}&\rho h\ddot{w}+2\rho h\Omega(\dot{w}'-\dot{u})-\rho h\Omega^2(w+2u'-w'')+\tfrac{D}{R^4}(w''''-u''')+\\&\tfrac{K}{R^2}(w+u')+\tfrac{\sigma_\theta^0 h}{R^2}(u'-w'')+k_r w=-P(\theta,t),\\&\rho h\ddot{u}+2\rho h\Omega(\dot{u}'+\dot{w})-\rho h\Omega^2(u-2w'-u'')+\tfrac{D}{R^4}(w'''-u'')-\\&\tfrac{K}{R^2}(w'+u'')+\tfrac{\sigma_\theta^0 h}{R^2}(u-w')+k_c u=0.\end{aligned} \tag{14}$$

where $D=Eh^3/12$ is the bending stiffness, $K=Eh$ is the membrane stiffness. σ_θ^0 is the initial hoop stress caused by rotation given by

$$\sigma_\theta^0=\frac{\rho R^2\Omega^2}{1+k_r R^2/K-\rho R^2\Omega^2/E}. \tag{15}$$

The periodicity conditions must be satisfied:

$$w(0,t)=w(2\pi,t),\ u(0,t)=u(2\pi,t). \tag{16}$$

Eqs. (14)–(16) complete the description of the problem using the classical thin ring model.

Eq. (14) can be rewritten in dimensionless form as

$$\begin{aligned}&W_{,\tau\tau}+W_{,\bar{\theta}\bar{\theta}\bar{\theta}\bar{\theta}}+(\bar{N}+\bar{v}^2)W_{,\bar{\theta}\bar{\theta}}+(\bar{k}^2+\bar{k}_r-\bar{k}^2\bar{v}^2)W+2\bar{v}W_{,\bar{\theta}\bar{\tau}}\\&\quad-\bar{k}U_{,\bar{\theta}\bar{\theta}\bar{\theta}}+(\bar{k}+\bar{k}\bar{N}-2\bar{k}\bar{v}^2)U_{,\bar{\theta}}-2\bar{k}\bar{v}U_{,\tau}=-\bar{P}(\bar{\theta},\tau),\\&U_{,\tau\tau}-(\bar{k}^2+1-\bar{v}^2)U_{,\bar{\theta}\bar{\theta}}+(\bar{k}_c-\bar{k}^2\bar{v}^2+\bar{k}^2\bar{N})U+2\bar{v}U_{,\bar{\theta}\tau}+\bar{k}W_{,\bar{\theta}\bar{\theta}\bar{\theta}}\\&\quad-(\bar{k}+\bar{k}\bar{N}-2\bar{k}\bar{v}^2)W_{,\bar{\theta}}+2\bar{k}\bar{v}W_{,\tau}=0\end{aligned} \tag{17}$$

using the same dimensionless parameters introduced in Eq. (11). The subscripts "$\bar{\theta}$" and "τ" denote derivatives with respect these variables. $\bar{P}$ is the dimensionless force. The dimensionless hoop tension is given by

$$\bar{N}=\frac{\bar{v}^2\bar{k}^2}{\bar{k}^2+\bar{k}_r-\bar{v}^2\bar{k}^2}. \tag{18}$$

In Eq. (17) only low order terms (the displacements at the middle surface of the ring) remain, i.e.

$$W(\bar{\theta},\tau)=w_0(\theta,t)/R,\ U(\bar{\theta},\tau)=u_0(\theta,t)/R. \tag{19}$$

The dispersion relation of the classical model in the space-fixed coordinate system is

$$\begin{aligned}&(\bar{\omega}^2-\bar{k}^2-\bar{\gamma}^4-\bar{k}_r+\bar{v}^2\bar{k}^2-\bar{N}\bar{\gamma}^2+\bar{v}^2\bar{\gamma}^2+2\bar{v}\bar{\omega}\bar{\gamma})\\&\quad\times(\bar{\omega}^2-\bar{\gamma}^2-\bar{k}^2\bar{\gamma}^2-\bar{k}_c+\bar{v}^2\bar{k}^2-\bar{N}\bar{k}^2+\bar{v}^2\bar{\gamma}^2+2\bar{v}\bar{\omega}\bar{\gamma})\\&\quad-(\bar{k}\bar{\gamma}^3+\bar{k}\bar{\gamma}+\bar{k}\bar{\gamma}\bar{N}-2\bar{v}\bar{k}\bar{\omega}-2\bar{v}^2\bar{\gamma}\bar{k})^2=0.\end{aligned} \tag{20}$$

which is obtained by substituting

$$W(\bar{\theta},\tau)=A\mathrm{e}^{\mathrm{i}\bar{\gamma}\bar{\theta}+\mathrm{i}\bar{\omega}\tau},\quad U(\bar{\theta},\tau)=B\mathrm{e}^{\mathrm{i}\bar{\gamma}\bar{\theta}+\mathrm{i}\bar{\omega}\tau} \tag{21}$$

into the homogeneous part of Eq. (17) and taking the determinant of the coefficient matrix.

2.3. The method of the images: application to a point (line) load

In engineering practice, the load applied to a rotating ring is very often assumed as a point load, e.g. the tyre-ground contact load to a pneumatic tire (Padovan, 1976) and the wheel-rail contact load to a flexible train wheel (Metrikine and Tochilin, 2000). In this section, the dynamic response of a rotating ring subjected to a stationary point load of harmonically varying amplitude is considered. In plane strain assumption, the point load is actually a line load distributed along the width of the ring. Assuming further that the load is applied at $\theta=0$ and $P(\theta,t)=P_0\exp(\mathrm{i}\Omega_\mathrm{f}t)\,\delta((R+h/2)\theta)$. Eq. (2) then reads

$$\begin{aligned}&\overset{\text{variation}}{\downarrow}\\&=b\int_{t_1}^{t_2}\int_0^{2\pi}\left(P(\theta,t)\,\delta\left(w\,|_{z=h/2}\right)(R+h/2)\right)\mathrm{d}\theta\mathrm{d}t.\end{aligned} \tag{22}$$

The dimension of P_0 is $\mathrm{N.m}^{--1}$ and δ is the Dirac delta function. The right hand side of Eq. (5) becomes

$$\begin{aligned}&\int_{-\frac{h}{2}}^{\frac{h}{2}}\left(\mathrm{I}_1^{\mathrm{lin}}z^l\right)\mathrm{d}z+\rho\int_{-\frac{h}{2}}^{\frac{h}{2}}\left(r(\dot{v}_1+\Omega v_1'-\Omega v_2)z^l\right)\mathrm{d}z\\&\quad+\left(f_1^{\mathrm{lin}}-f_2^{\mathrm{lin}}(-1)^l\right)\left(\tfrac{h}{2}\right)^l\\&\quad=-\left(\tfrac{h}{2}\right)^l P_0\exp(\mathrm{i}\Omega_\mathrm{f}t)\delta(\theta),\ (l=0,1,2,3\ldots N_1).\end{aligned} \tag{23}$$

whereas the first equation of Eq. (14) reads

$$\begin{aligned}&\rho h\ddot{w}+2\rho h\Omega(\dot{w}'-\dot{u})-\rho h\Omega^2(w+2u'-w'')+\tfrac{D}{R^4}(w''''-u''')\\&\quad+\tfrac{K}{R^2}(w+u')+\tfrac{\sigma_\theta^0 h}{R^2}(u'-w'')+k_r w=-\tfrac{P_0\exp(\mathrm{i}\Omega_\mathrm{f}t)}{R}\delta(\theta).\end{aligned} \tag{24}$$

The method of the images has been first applied to study the steady-state response of an elastic ring subjected to a moving load in Metrikine and Tochilin (2000). The idea of this method is that the response of a bounded (in our case ring-like) system to a single load is equivalent in the linear framework to the response of a part of an infinitely long system (described by the same equations) subjected to an infinite set of loads. In other words, the method utilizes the fact that the periodic boundary conditions are satisfied by introducing additional loads as shown in Fig. 2. These loads are called images since their locations are normally mirrored to the real load with respect to the boundaries. In the considered case, to satisfy the periodicity of the displacements, one should introduce infinitely many equivalent loads at a fixed distance 2π from each other. By doing so, Eq. (23) can be rewritten as

$$\begin{aligned}&\int_{-\frac{h}{2}}^{\frac{h}{2}}\left(\mathrm{I}_1^{\mathrm{lin}}z^l\right)\mathrm{d}z+\rho\int_{-\frac{h}{2}}^{\frac{h}{2}}\left(r(\dot{v}_1+\Omega v_1'-\Omega v_2)z^l\right)\mathrm{d}z\\&\quad+\left(f_1^{\mathrm{lin}}-f_2^{\mathrm{lin}}(-1)^l\right)\left(\tfrac{h}{2}\right)^l=-P_0\exp(\mathrm{i}\Omega_\mathrm{f}t)\left(\tfrac{h}{2}\right)^l\sum_{j=-\infty}^{+\infty}\delta(\theta+2\pi j),\\&\quad(l=0,1,2,3\ldots N_1).\end{aligned} \tag{25}$$

The linearised equations of motion in the circumferential direction, namely Eq. (6) remains unchanged. In Eq. (25), the periodicity condition Eq. (7) is now captured by the summation of infinitely many equidistant loads. Due to complexity, the dimensionless forms of Eqs. (25) and (6) from the high-order model are not explicitly given here.

The stationary line load along the width in the plane strain high-order model degenerates to a point load in the classical low-order rotating thin ring model. Performing similar derivations for the classical model, the first equation in Eq. (17) becomes

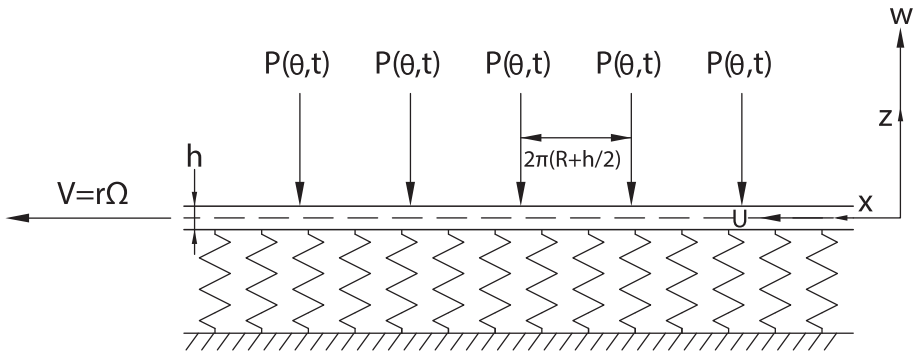

Fig. 2. Method of the images for an axially moving "extended ring".

$$W_{,\tau\tau}+W_{,\bar\theta\bar\theta\bar\theta\bar\theta}+(\bar N+\bar v^2)W_{,\bar\theta\bar\theta}+(\bar k^2+\bar k_r-\bar k^2\bar v^2)W+2\bar vW_{,\bar\theta\tau}-\bar kU_{,\bar\theta\bar\theta\bar\theta}$$
$$+(\bar k+\bar k\bar N-2\bar k\bar v^2)U_{,\bar\theta}-2\bar k\bar vU_{,\tau}=-\bar P_0\exp(\mathrm{i}\bar\Omega_{\mathrm f}\tau)\sum_{j=-\infty}^{+\infty}\delta(\bar\theta+2\pi j/\bar k) \tag{26}$$

in which the periodicity condition is enforced by a summation of infinitely many loads. In addition, $\bar\Omega_{\mathrm f}=\Omega_{\mathrm f}k/c_0$ is the dimensionless frequency of the load and $\bar P_0=P_0\bar k/(Eh)$ is the dimensionless load amplitude.

Since the problem is linear, the exact solution is the summation of the responses to all the individual loads and all the loads generate equivalent displacement fields but with a spatial shift. More specifically, it suffices to obtain the response of the axially moving "extended ring" to a single load and then sum up this response infinitely many times accounting for the spatial shift 2π. One of the main advantages of the method of the images is that the aforementioned infinite summation can be computed analytically, using the formulae of an infinite geometric progression (Metrikine and Tochilin, 2000).

Considering a single load, the dimensionless form of Eqs. (25) and (6) can be solved by means of application of the integral Fourier transform. Defining this transform as

$$\begin{Bmatrix}\tilde{\tilde W}_l^{\bar\omega,\bar\gamma}\\ \tilde{\tilde U}_q^{\bar\omega,\bar\gamma}\end{Bmatrix}=\int_{-\infty}^{+\infty}\int_{-\infty}^{+\infty}\begin{Bmatrix}W_l\\U_q\end{Bmatrix}\exp(-\mathrm{i}\bar\gamma\bar\theta-\mathrm{i}\bar\omega\tau)\mathrm d\tau\mathrm d\bar\theta \tag{27}$$

where $\mathrm{i}=\sqrt{-1}$ and $\bar\gamma,\bar\omega,\bar\theta,\tau$ are defined in Eq. (11). Applying the above transformation to the dimensionless form of Eqs. (25) and (6), one obtains a set of algebraic equations

$$\mathbf{Ca}=\mathbf{f} \tag{28}$$

in which $\mathbf{C}$ is the coefficient matrix, $\mathbf{a}$ is the displacement vector and $\mathbf{f}$ is the force vector. The matrix and vectors are given in Appendix C.

All the unknown displacement components can be solved for using the Cramer's rule, i.e.

$$\begin{aligned}\tilde{\tilde W}_l^{\bar\omega,\bar\gamma}&=\frac{\det(\mathbf C_l)}{\det(\mathbf C)}=\frac{2\pi\bar P_0\delta(\bar\omega-\bar\Omega_{\mathrm f})\Delta_{wl}}{\Delta}\\ \tilde{\tilde U}_q^{\bar\omega,\bar\gamma}&=\frac{\det(\mathbf C_{N_1+1+q})}{\det(\mathbf C)}=\frac{2\pi\bar P_0\delta(\bar\omega-\bar\Omega_{\mathrm f})\Delta_{uq}}{\Delta}\end{aligned} \tag{29}$$

Matrix $\mathbf{C}_l$ is formed by replacing the lth column of $\mathbf{C}$ by the force vector $\mathbf{f}$ whereas $\mathbf{C}_{N_1+1+q}$ is the matrix $\mathbf{C}$ whose (N_1+1+q)th column is replaced by $\mathbf{f}$. The expressions Δ,Δ_{wl} and Δ_{uq} can be obtained by using any symbolic computation software. In addition,

$$\Delta=\det(\mathbf C) \tag{30}$$

is the dispersion relation of the rotating ring using the high-order model.

The next step is to invert the obtained solutions Eq. (29) to the time and space domain by using the inverse Fourier transform (Metrikine and Tochilin, 2000):

$$\begin{aligned}W_l^s(\bar\theta,\tau)&=\frac{\bar P_0}{2\pi}\exp(\mathrm{i}\bar\Omega_{\mathrm f}\tau)\int_{-\infty}^{+\infty}\frac{\Delta_{wl}(\bar\Omega_{\mathrm f},\bar\gamma)}{\Delta(\bar\Omega_{\mathrm f},\bar\gamma)}\exp(\mathrm{i}\bar\gamma\bar\theta)\mathrm d\bar\gamma\\ U_q^s(\bar\theta,\tau)&=\frac{\bar P_0}{2\pi}\exp(\mathrm{i}\bar\Omega_{\mathrm f}\tau)\int_{-\infty}^{+\infty}\frac{\Delta_{uq}(\bar\Omega_{\mathrm f},\bar\gamma)}{\Delta(\bar\Omega_{\mathrm f},\bar\gamma)}\exp(\mathrm{i}\bar\gamma\bar\theta)\mathrm d\bar\gamma\end{aligned} \tag{31}$$

where $\bar\theta$ is the distance from the load. The integral in Eq. (31) can be evaluated by employing the residue theorem (the superscript "s" stands for single load):

$$W_l^s(\bar\theta,\tau)=\begin{cases}\mathrm{i}\bar P_0\exp(\mathrm{i}\bar\Omega_{\mathrm f}\tau)\sum_p B_{wl}^p\exp(\mathrm{i}\bar\gamma_p\bar\theta) & \text{if}\quad\bar\theta>0\\ -\mathrm{i}\bar P_0\exp(\mathrm{i}\bar\Omega_{\mathrm f}\tau)\sum_n B_{wl}^n\exp(\mathrm{i}\bar\gamma_n\bar\theta) & \text{if}\quad\bar\theta<0\end{cases} \tag{32}$$

$$U_q^s(\bar\theta,\tau)=\begin{cases}\mathrm{i}\bar P_0\exp(\mathrm{i}\bar\Omega_{\mathrm f}\tau)\sum_p B_{uq}^p\exp(\mathrm{i}\bar\gamma_p\bar\theta) & \text{if}\quad\bar\theta>0\\ -\mathrm{i}\bar P_0\exp(\mathrm{i}\bar\Omega_{\mathrm f}\tau)\sum_n B_{uq}^n\exp(\mathrm{i}\bar\gamma_n\bar\theta) & \text{if}\quad\bar\theta<0\end{cases} \tag{33}$$

in which:

$$\begin{aligned}B_{wl}^p&=\frac{\Delta_{wl}(\bar\Omega_{\mathrm f},\bar\gamma_p)}{\frac{\partial}{\partial\bar\gamma}(\Delta(\bar\Omega_{\mathrm f},\bar\gamma))|_{\bar\gamma=\bar\gamma_p}},\quad B_{uq}^p=\frac{\Delta_{uq}(\bar\Omega_{\mathrm f},\bar\gamma_p)}{\frac{\partial}{\partial\bar\gamma}(\Delta(\bar\Omega_{\mathrm f},\bar\gamma))|_{\bar\gamma=\bar\gamma_p}},\\ B_{wl}^n&=\frac{\Delta_{wl}(\bar\Omega_{\mathrm f},\bar\gamma_n)}{\frac{\partial}{\partial\bar\gamma}(\Delta(\bar\Omega_{\mathrm f},\bar\gamma))|_{\bar\gamma=\bar\gamma_n}},\quad B_{uq}^n=\frac{\Delta_{uq}(\bar\Omega_{\mathrm f},\bar\gamma_n)}{\frac{\partial}{\partial\bar\gamma}(\Delta(\bar\Omega_{\mathrm f},\bar\gamma))|_{\bar\gamma=\bar\gamma_n}}.\end{aligned} \tag{34}$$

$\bar\gamma_n$ denotes the roots of equation $\Delta(\bar\Omega_{\mathrm f},\bar\gamma)=0$ with negative imaginary part, whereas $\bar\gamma_p$ denotes the roots of the same equation with positive imaginary part.

After obtaining the solutions in the time domain for the single load case, the exact solution can be found as an infinite summation of terms with the spatial shift 2π, namely

$$\begin{aligned}W_l(\bar\theta,\tau)&=\sum_{j=-\infty}^{+\infty}W_l^s(\bar\theta+2\pi j/\bar k,\tau),\quad U_q(\bar\theta,\tau)\\ &=\sum_{j=-\infty}^{+\infty}U_q^s(\bar\theta+2\pi j/\bar k,\tau).\end{aligned} \tag{35}$$

Substituting Eqs. 32,33 into Eq. (35), both $W_l(\bar\theta,\tau)$ and $U_q(\bar\theta,\tau)$ consist of a sum of a geometric progression with infinite number of terms. Following the same procedure as in Metrikine and Tochilin (2000), the summation can be further simplified and the analytical expressions of the displacements of the ring can be derived as (Metrikine and Tochilin, 2000)

$$W_l(\bar{\theta},\tau)=\begin{cases}\mathrm{i}\bar{P}_0\left[\sum_p B_{wl}^p\frac{\exp(\mathrm{i}\bar{\gamma}_p\bar{\theta})}{1-\exp(\mathrm{i}2\pi\bar{\gamma}_p/\bar{k})}\right.\\ \left.-\sum_n B_{wl}^n\frac{\exp(\mathrm{i}\bar{\gamma}_n(\bar{\theta}-2\pi/\bar{k}))}{1-\exp(-\mathrm{i}2\pi\bar{\gamma}_n/\bar{k})}\right]\exp(\mathrm{i}\bar{\Omega}_\mathrm{f}\tau) & \text{if}\quad \pi/\bar{k}>\bar{\theta}>0\\ \mathrm{i}\bar{P}_0\left[\sum_p B_{wl}^p\frac{\exp(\mathrm{i}\bar{\gamma}_p(\bar{\theta}+2\pi/\bar{k}))}{1-\exp(\mathrm{i}2\pi\bar{\gamma}_p/\bar{k})}\right.\\ \left.-\sum_n B_{wl}^n\frac{\exp(\mathrm{i}\bar{\gamma}_n\bar{\theta})}{1-\exp(-\mathrm{i}2\pi\bar{\gamma}_n/\bar{k})}\right]\exp(\mathrm{i}\bar{\Omega}_\mathrm{f}\tau) & \text{if}\quad -\pi/\bar{k}<\bar{\theta}<0\end{cases}\tag{36}$$

$$U_q(\bar{\theta},\tau)=\begin{cases}\mathrm{i}\bar{P}_0\left[\sum_p B_{uq}^p\frac{\exp(\mathrm{i}\bar{\gamma}_p\bar{\theta})}{1-\exp(\mathrm{i}2\pi\bar{\gamma}_p/\bar{k})}\right.\\ \left.-\sum_n B_{uq}^n\frac{\exp(\mathrm{i}\bar{\gamma}_n(\bar{\theta}-2\pi/\bar{k}))}{1-\exp(-\mathrm{i}2\pi\bar{\gamma}_n/\bar{k})}\right]\exp(\mathrm{i}\bar{\Omega}_\mathrm{f}\tau) & \text{if}\quad \pi/\bar{k}>\bar{\theta}>0\\ \mathrm{i}\bar{P}_0\left[\sum_p B_{uq}^p\frac{\exp(\mathrm{i}\bar{\gamma}_p(\bar{\theta}+2\pi/\bar{k}))}{1-\exp(\mathrm{i}2\pi\bar{\gamma}_p/\bar{k})}\right.\\ \left.-\sum_n B_{uq}^n\frac{\exp(\mathrm{i}\bar{\gamma}_n\bar{\theta})}{1-\exp(-\mathrm{i}2\pi\bar{\gamma}_n/\bar{k})}\right]\exp(\mathrm{i}\bar{\Omega}_\mathrm{f}\tau) & \text{if}\quad -\pi/\bar{k}<\bar{\theta}<0\end{cases}\tag{37}$$

The real part of the above-given solution should be taken if the time signature of the load is given as $P(t)=P_0\cos(\Omega_\mathrm{f}t)$, whereas the imaginary part corresponds to $P(t)=P_0\sin(\Omega_\mathrm{f}t)$. The total dimensionless displacements are

$$W(\bar{z},\bar{\theta},\bar{\tau})=\sum_{l=0}^{N_1}(\bar{z}^l W_l(\bar{\theta},\bar{\tau})),\ U(\bar{z},\bar{\theta},\bar{\tau})=\sum_{q=0}^{N_2}(\bar{z}^q U_q(\bar{\theta},\bar{\tau})).\tag{38}$$

2.4. Approximation of the Dirac function by Gaussian distribution

When a line load along the out-of-plane direction is applied to a two-dimensional elastic medium, the assumptions of linear elasticity are inevitably violated in the vicinity of the loading point (Murakami, 2016), as well as for the high-order theory presented here. This is an intrinsic problem of this type of higher-order theories, not only for rings, but also for shells, beams, etc. and for both static and dynamic loads. For stiff rings (soft foundation), such as rings made of steel, the sharp changes at the loading point of higher order terms are not obvious. This is due to the fact that the deformation caused by the concentrated force is balanced primarily by the foundation (the excitation of $n=1$ mode as will be shown in the following section). For soft rings (stiff foundation), the force causes much greater elastic deformations in the ring than the deformation of the foundation. Therefore, the violation becomes apparent. In order to circumvent this problem, one may realistically assume that a contact patch exists on the ring and thus distributed forces are applied on the ring. A Gaussian distribution can be used to specify the distribution of tractions within the contact patch. The displacements under the loading position become smooth if a distributed force is applied instead of a concentrated one. Using a normalized Gaussian distribution, the load represented by Dirac function can be replaced by a distributed load in the following manner:

$$\begin{aligned}P(t)\delta(\theta)&=\frac{P(t)}{\sqrt{2\pi\sigma^2}}\exp\left(-\frac{\theta^2}{2\sigma^2}\right)\\&=\frac{P_0\exp(\mathrm{i}\Omega_\mathrm{f}t)}{\sqrt{2\pi\sigma^2}}\exp\left(-\frac{\theta^2}{2\sigma^2}\right).\end{aligned}\tag{39}$$

The integrals of the left-hand side and right-hand side of Eq. (39) from $-\pi$ to π both equal to $P(t)$. Consequently, Eq. (31), namely the dynamic response of the ring under a single load, becomes

$$\begin{aligned}W_l^s(\bar{\theta},\tau)&=\tfrac{1}{2\pi}\exp(\mathrm{i}\bar{\Omega}_\mathrm{f}\tau)\int_{-\infty}^{+\infty}\frac{\bar{P}(\bar{\gamma})\Delta_{wl}(\bar{\Omega}_\mathrm{f},\bar{\gamma})}{\Delta(\bar{\Omega}_\mathrm{f},\bar{\gamma})}\exp(\mathrm{i}\bar{\gamma}\bar{\theta})\mathrm{d}\bar{\gamma}\\ U_q^s(\bar{\theta},\tau)&=\tfrac{1}{2\pi}\exp(\mathrm{i}\bar{\Omega}_\mathrm{f}\tau)\int_{-\infty}^{+\infty}\frac{\bar{P}(\bar{\gamma})\Delta_{uq}(\bar{\Omega}_\mathrm{f},\bar{\gamma})}{\Delta(\bar{\Omega}_\mathrm{f},\bar{\gamma})}\exp(\mathrm{i}\bar{\gamma}\bar{\theta})\mathrm{d}\bar{\gamma}\end{aligned}\tag{40}$$

where $\bar{P}(\bar{\gamma})$ is the dimensionless form of the Fourier transform of

$$\frac{P_0}{\sqrt{2\pi\sigma^2}}\exp\left(-\frac{\theta^2}{2\sigma^2}\right)\tag{41}$$

in the wavenumber domain. Eq. (40) can be evaluated by direct numerical integration considering proper truncation of $\bar{\gamma}$ to obtain convergent results. After obtaining the dynamic response of the ring to a single load, the total response is given similarly to Eq. (35) by proper truncation of the number of images (mirrored load). Note that the dynamic responses caused by any form of distributed loads can be solved in the same manner as the load of Gaussian distribution.

2.5. Consideration of damping

The energy dissipation in the rotating ring can be considered in two ways. One way is to treat the foundation as Kelvin–Voigt ele-

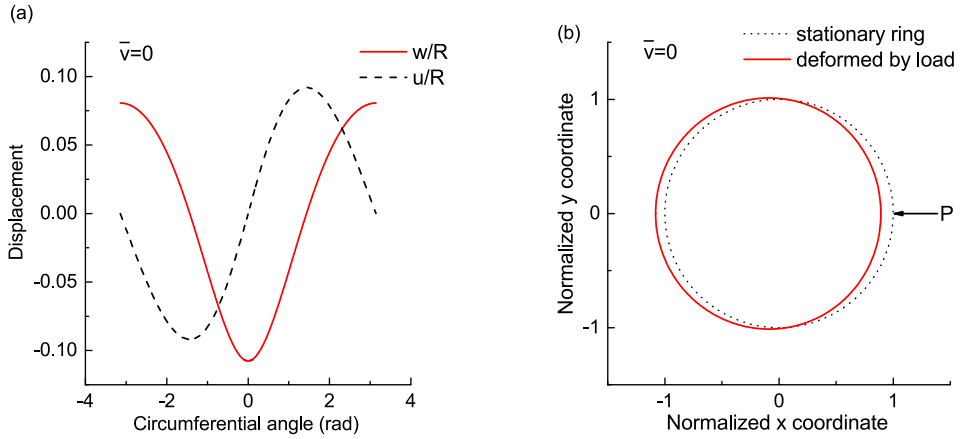

Fig. 3. Classical model, $\bar{v}=0,\bar{k}_r=1\times10^{-6},\bar{k}_c=1\times10^{-9}$: (a) Displacements; (b) Ring shape.

ments with spring and dashpot in parallel. In this case, one can include the viscous damping of the foundation directly by replacing

$$k_r \to k_r + \sigma_w\left(\frac{\partial}{\partial t} + \Omega\frac{\partial}{\partial\theta}\right),\ k_c \to k_c + \sigma_u\left(\frac{\partial}{\partial t} + \Omega\frac{\partial}{\partial\theta}\right). \tag{42}$$

Another dissipation mechanism is the internal damping in the ring material. When one considers high values of $\bar{k}_r$ (stiff foundation), one is equivalently considering soft materials like rubbers and polymers. In this case, one needs to take into account their viscoelastic properties since the energy is dissipated mainly by the material itself. To this end, the following internal damping is introduced:

$$E^* = E(1 + \zeta(\partial/\partial t + \Omega\partial/\partial\theta)) \tag{43}$$

where ζ is the hysteresis loss factor of the material. The shear modulus changes accordingly to

$$G^* = \frac{E^*}{2(1+\nu)} = G(1 + \zeta(\partial/\partial t + \Omega\partial/\partial\theta)). \tag{44}$$

The Lamé constants can be obtained accordingly.

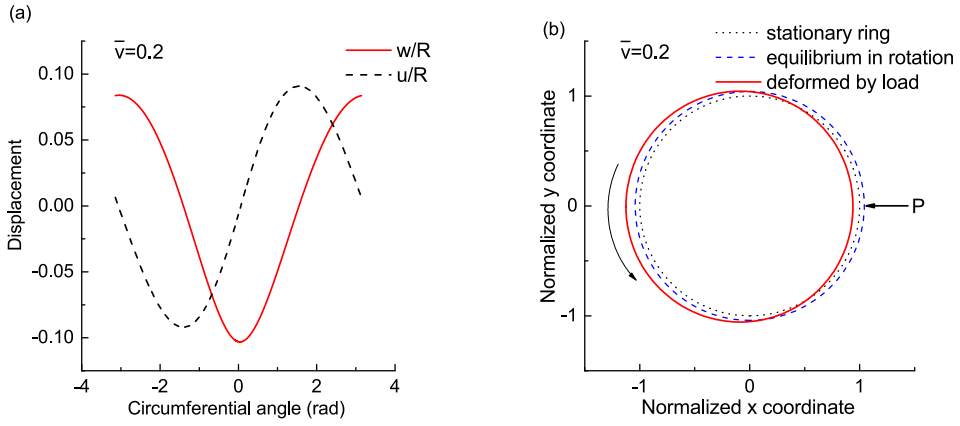

Fig. 4. Classical model, $\bar{\nu} = 0.2, \bar{k}_r = 1\times10^{-6}, \bar{k}_c = 1\times10^{-9}$: (a) Displacements; (b) Ring shape.

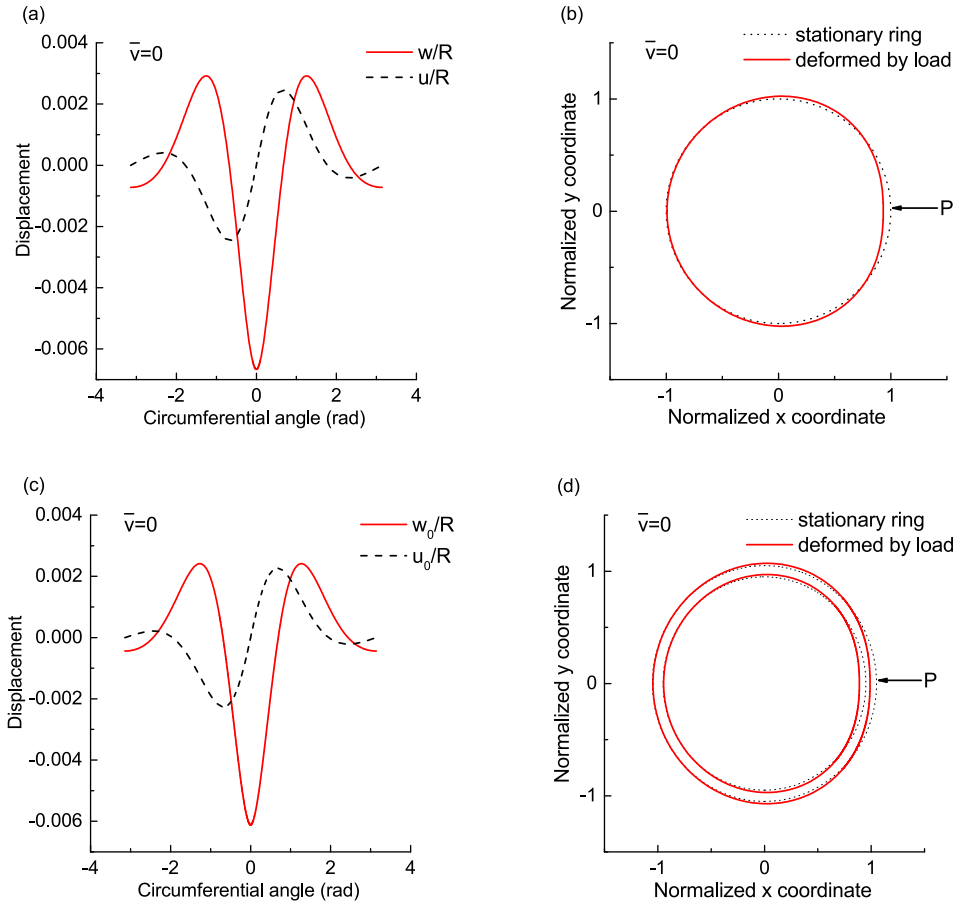

Fig. 5. Displacements and deformation patterns of the ring for $\bar{k}_r = 1\times10^{-6}, \bar{k}_c = 1\times10^{-4}$ and $\bar{\nu} = 0$ resulting from: (a) and (b) Classical model; (c) and (d) High-order model (only the displacements at middle surface are shown). The ring shapes are scaled by 10.

3. Steady-state response of a rotating ring under a stationary line (point) load

The steady-state response of a rotating ring under a stationary load is studied in this section for different system parameters. It has been shown in Lu et al. (2019) that the in-plane free vibrations of a rotating ring can be unstable. Therefore the parameters of the ring-foundation system are chosen such that the free vibrations are always stable at the rotational speeds which are of interests and therefore the steady-state response exists. The dimensionless parameters $\bar{k}_r$ and $\bar{k}_c$ which represent the ratios of the stiffness of the foundation to the stiffness of the ring itself are of significant importance. Low values of $\bar{k}_r$ and $\bar{k}_c$ imply that the ring itself is stiff compared to the elastic foundation, for example, a steel ring. In contrast, high values of $\bar{k}_r$ and $\bar{k}_c$ indicate that the ring is soft in comparison with the elastic foundation, for example, a ring made of rubber-like material. In the following, the steady-state responses of the two configurations are investigated. In the sequel, $N_1 = N_2 = 5$ are chosen for truncating the displacement field expansions in Eq. (3). The convergence of this choice has been tested.

3.1. Soft foundation (stiff ring)

A ring supported by soft springs can correspond to the case that the foundation flexibility is high comparing to that of the ring. In this subsection, the following dimensionless parameters are chosen: $\bar{k}_r = 1 \times 10^{-6}$, $\kappa = h/R = 0.1$, $\bar{P}_0 = 1 \times 10^{-5}$. The ring is assumed to rest on a viscoelastic foundation, see Eq. (42). A coefficient ξ is introduced to represent the ratio of the viscous damping to the stiffness of the foundation. The ratios are defined as follows:

$$\xi_w = \frac{\sigma_w}{k_r}, \quad \xi_u = \frac{\sigma_u}{k_c}. \tag{45}$$

For simplicity, the same ratio is applied in both the radial and circumferential directions, namely $\xi_w = \xi_u = \xi = 5 \times 10^{-3} s$. The Poisson's ratio is chosen to be $\nu = 0.3$ which refers to a steel ring.

The steady-state response predicted by the classical model is studied first. Fig. 3 shows the static response of a stationary ring subjected to a radial point load with constant magnitude according to the classical model Eq. (14). Fig. 4 shows the quasi-static response of the same ring subjected to the same load; but now the ring rotates at $\bar{v} = 0.2$. From Fig. 3, it can be seen that the circumferential displacement is almost a perfect sinus, whereas the radial displacement is of a cosinusoidal shape. The ring exhibits a translational rigid body-like motion in the direction of the applied force governed mainly by the $n = 1$ mode. As for $\bar{v} = 0.2$, the ring experiences a static radial expansion caused by rotation. The response is still mainly governed by the $n = 1$ mode. In this case, predictions of the high-order model are not shown because the responses calculated from the classical model and the high-order model are very similar; the responses predicted by the high-order model are just slightly smaller. When the applied load is varying harmonically, e.g. $\bar{P}(\tau) = \bar{P}_0 \cos(\bar{\Omega}_f \tau)$, many higher modes can be excited. The difference between the classical model and the high-order model are more obvious in this case but still marginal provided that the frequency of excitation is about or lower than the first cut-off frequency of the system.

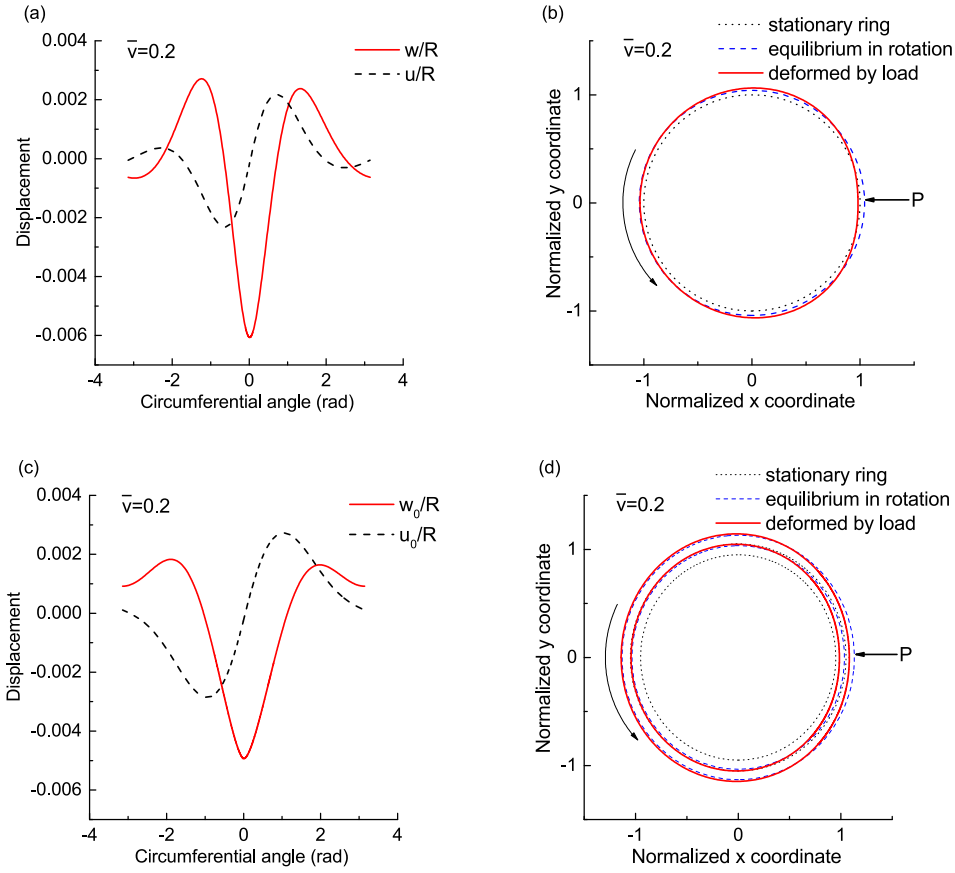

Fig. 6. Displacements and deformation patterns of the ring for $\bar{k}_r = 1 \times 10^{-6}, \bar{k}_c = 1 \times 10^{-4}$ and $\bar{v} = 0.2$ resulting from: (a) and (b) Classical model; (c) and (d) High-order model (only the displacements at middle surface are shown). The ring shapes are scaled by 10.

The influence of circumferential springs can be assessed by comparing Figs. 3–6. Higher $\bar{k}_c$ suppresses the responses in both the radial and circumferential directions effectively. As expected, the effect on circumferential displacement is more significant.

3.2. Stiff foundation (soft ring)

In this configuration, the material itself is soft relative to the foundation. Again $\kappa = h/R = 0.1$ is assumed and the Poisson's ratio is chosen to be $\nu = 0.4$. When soft materials like rubbers or polymers are considered, the viscoelastic properties are better captured by the loss factor of the material given by Eq. (43). Here $\zeta = 0.002$ is employed. In addition, $\bar{k}_c = 0.1, \bar{k}_r = 0.01$ are chosen to represent a stiff foundation. The resonance speeds corresponding to this set of parameters are discussed in Lu et al. (2019). It has been shown in Lu et al. (2019) that there exists a critical speed after which wave-like patterns occur for a rotating ring subjected to a stationary load with constant magnitude. The critical speed, namely the minimum resonance speed is about $\bar{v} = 0.5$ for the chosen parameters (Lu et al., 2019). The dimensionless magnitude of the force is selected to be $\bar{P}_0 = 0.002$. Hereafter, the point load is approximated by Gaussian distribution Eq. (39) with $\sigma = 0.01$.

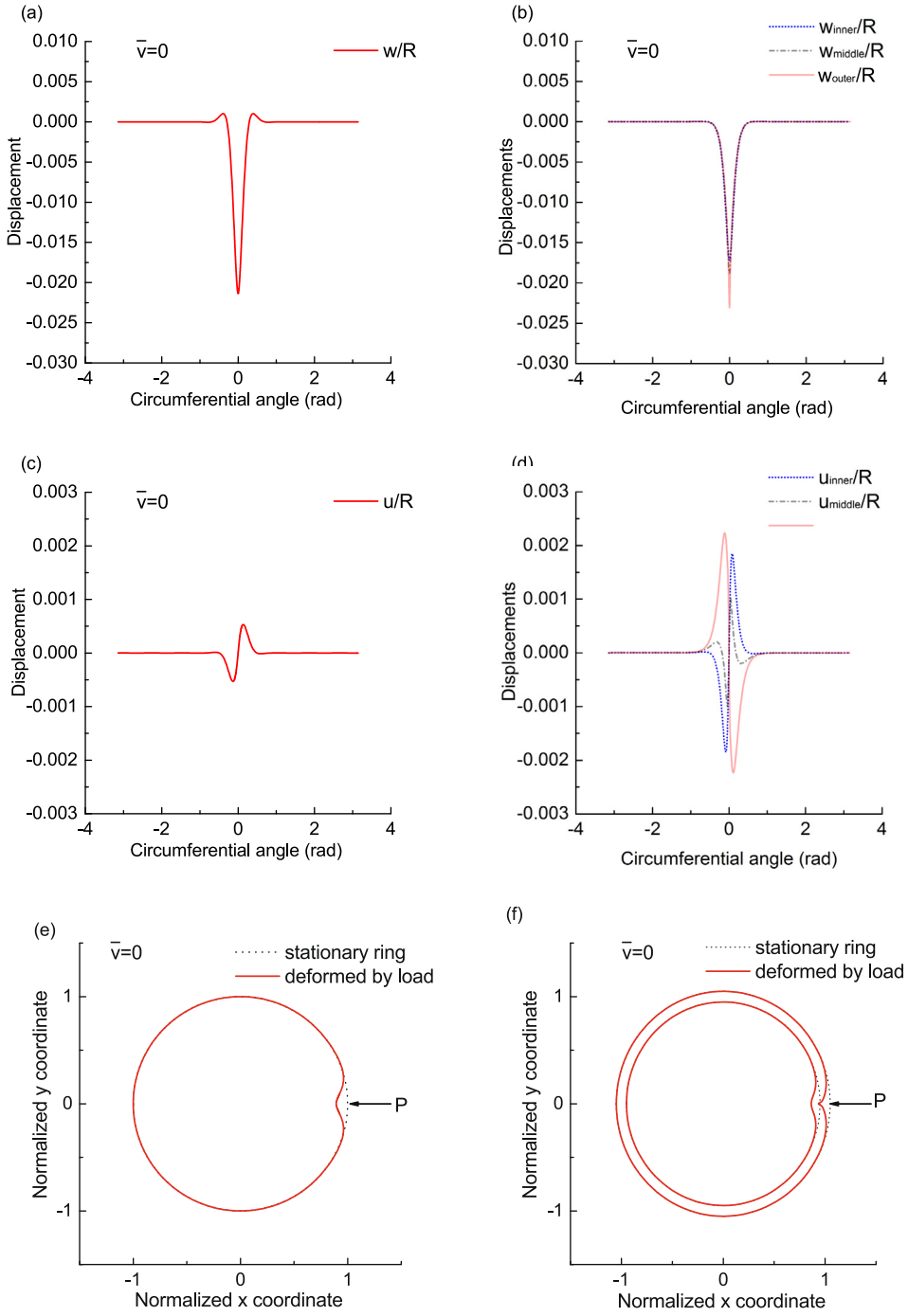

Fig. 7. Responses predicted using the classical (left) and high-order (right) models for $\bar{v} = 0, \bar{k}_r = 0.01, \bar{k}_c = 0.1$: (a) and (b) Radial displacements; (c) and (d) Circumferential displacements; (e) and (f) Ring deformation. The ring deformations are scaled by 5.

3.2.1. Dynamic response under a constant load

Fig. 7 presents the displacements and deformation patterns for $\bar{v} = 0$ (statics) using the classical and the high-order models. Only the middle surface displacements are predicted using the classical low-order model, whereas the displacements at the inner, middle and outer surfaces are shown for the high-order model hereafter. The through-thickness variation of the radial displacement is significant only in the vicinity of the loading area. The high-order model predicts greater circumferential displacement than that of the classical model. It is interesting to see that the circumferential displacement at the outer surface has a different sign than that at the middle and inner surfaces. The responses are localized around and symmetric with respect to the load in this static case as shown in Fig. 7(e) and (f).

Fig. 8 presents the displacements and deformations for a subcritical speed $\bar{v} = 0.3$ based on the classical model and the high-order model. The chosen rotational speed is lower than the critical speed related to resonances and thus no wave-like deformations are expected. The response of the ring rotating at $\bar{v} = 0.3$ is also localized, however it is not symmetric with respect to the load because of the effect of damping. The influence of higher order corrections is of significance now. As shown in Fig. 8(a) and (b), the high-order model results in smaller radial displacements. Although the circumferential displacements at the middle surface calculated using the classical and high-order model are similar, the circumferential displacements at the inner and outer surfaces are significantly larger than that at the middle surface computed from high-order model.

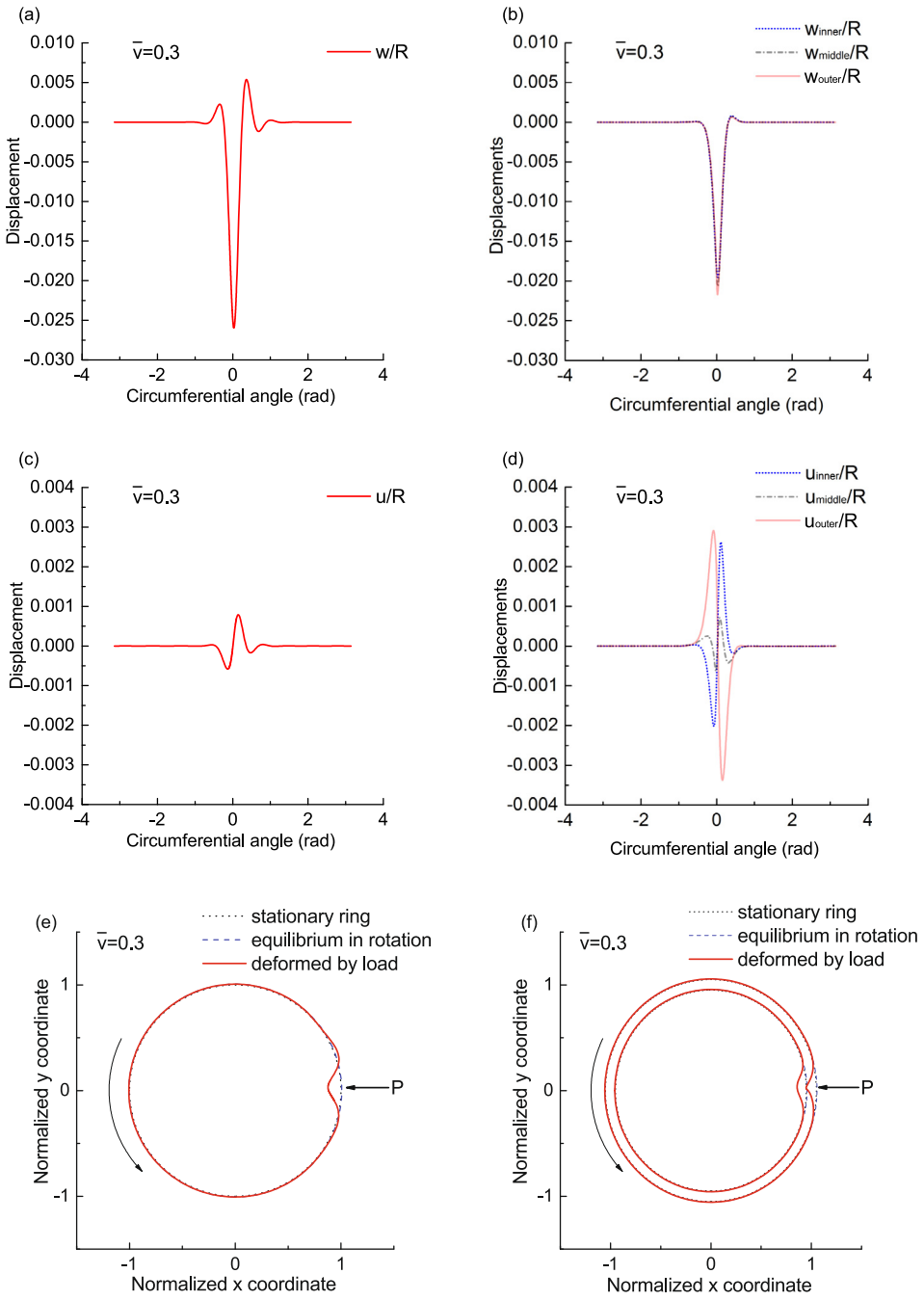

Fig. 8. Responses predicted using the classical (left) and high-order (right) models for $\bar{v} = 0.3, \bar{k}_r = 0.01, \bar{k}_c = 0.1$: (a) and (b) Radial displacements; (c) and (d) Circumferential displacements; (e) and (f) Ring deformation. The ring deformations are scaled by 5.

According to Lu et al. (2019), the ring rotates super-critically at speed $\bar{v} = 0.7$ since this speed is higher than the minimum resonance speed predicted both by the classical model and the high-order model. From Fig. 9(a-d), it can be seen that waves are generated in the ring that rotates with $\bar{v} = 0.7$. In the area which corresponds to negative circumferential angle (also called "leading edge" as defined in Chatterjee et al. (1999)) in Fig. 9, the waves are shorter, whereas waves have larger wavelengths in the area corresponding to positive circumferential angle (also called "trailing edge" as defined in Chatterjee et al. (1999)) in Fig. 9. When damping is small ($\zeta = 0.002$), the positive-travelling waves and the negative-travelling waves interfere as shown in (a) and (c) of Fig. 9 as predicted using the classical model.

A comparison of Fig. 9(a) and (c) with Fig. 9(b) and (d) shows that the higher order corrections play an important role in the steady-state response when the ring rotates at super-critical speeds. The high-order model predicts much smaller wave-like radial displacement with larger wavelengths in the trailing edge. Unlike the prediction using the classical model shown in Fig. 9 (e), it is clear from Fig. 9(f) that the response in the leading edge decays significantly. This is consistent with the experiments which were done for rolling tires, in which the stationary deformation patterns exist only in the trailing edge (Chatterjee et al., 1999; Cho et al., 2007). Note that for the chosen parameters, namely $\bar{k}_r = 0.01, \bar{k}_c = 0.1$, the steady-state responses predicted using the classical model and the high-order theory all show wave-like patterns

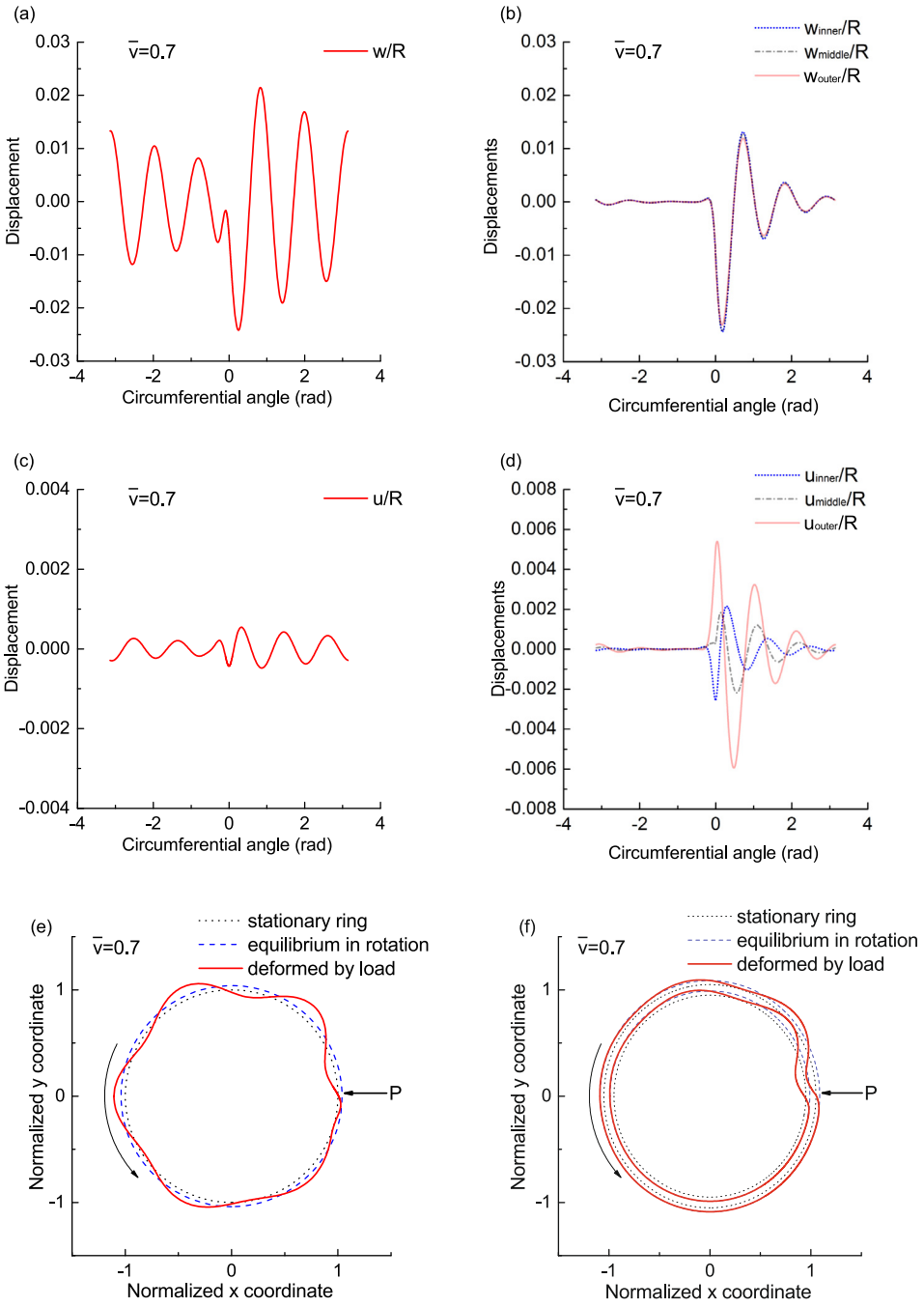

Fig. 9. Responses predicted using the classical (left) and high-order (right) models for $\bar{v} = 0.7, \bar{k}_r = 0.01, \bar{k}_c = 0.1$: (a) and (b) Radial displacements; (c) and (d) Circumferential displacements; (e) and (f) Ring deformation. The ring deformations are scaled by 5.

although the deformation patterns are significantly different. However, if other parameters are chosen the responses from both models can also differ largely. For example, as shown in Lu et al. (2019) the resonance speeds computed from the classical model and the high-order theory can be completely different and therefore the steady-state responses predicted by both models are expected to be distinct.

3.2.2. Dynamic response under a harmonic load

When considering the steady-state response of a rotating ring to a stationary harmonic point load, insights can be gained by analysing the dispersion curves obtained from the governing equations derived in a space-fixed coordinate system. The dispersion relations of the classical low-order model and the high-order model are given in Eqs. (20) and (30), respectively. Fig. 10 shows the dispersion curves of the same ring parameters as used above. The results are calculated for the three rotational speeds discussed previously. The dashed horizontal lines $\bar{\Omega}_f$ in Fig. 10 correspond to the excitation frequency of the load. This frequency determines the deformation patterns of the ring. One crossing point between this line and the dispersion curves means one wave excited. The following observations can be made:

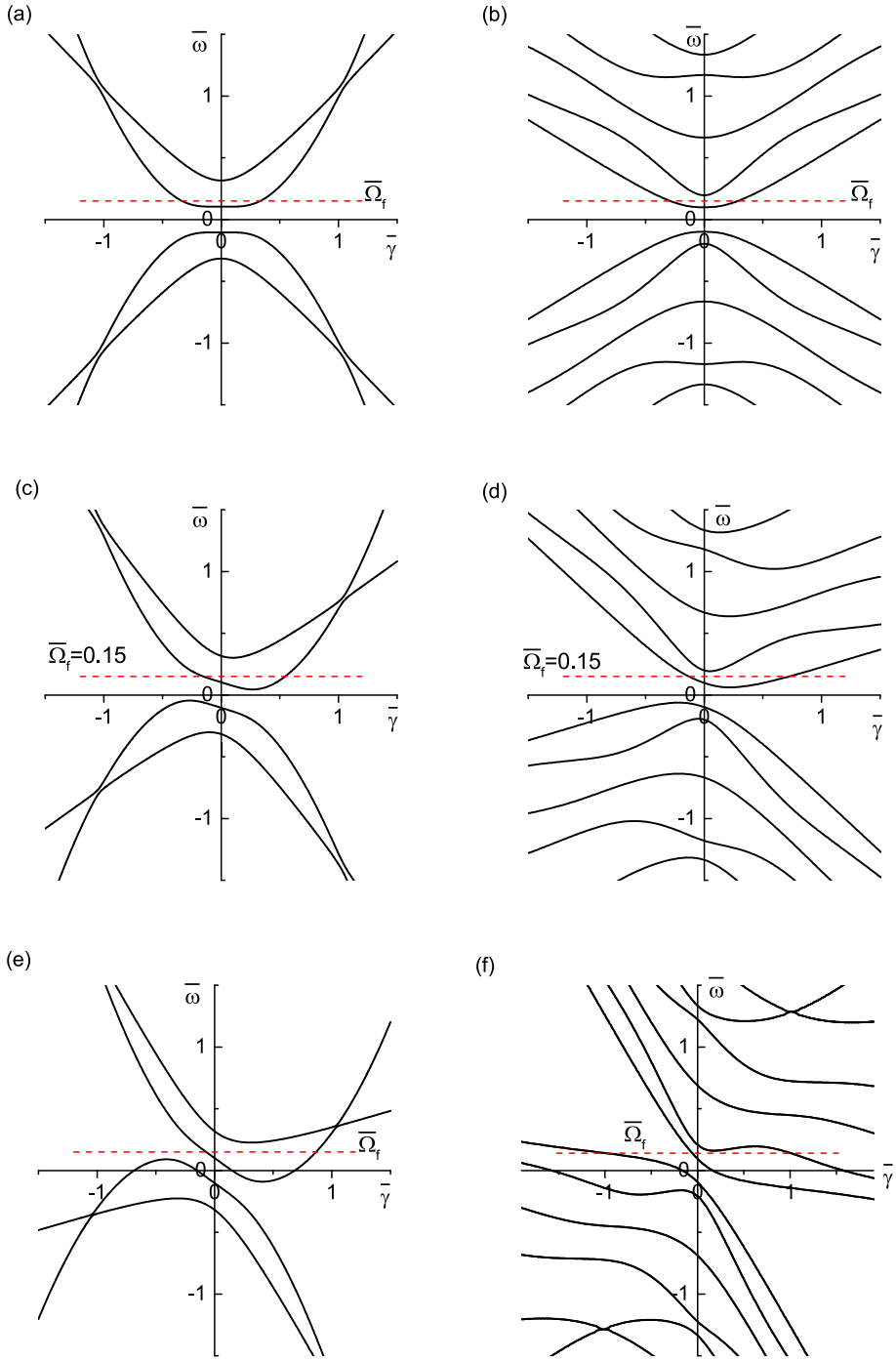

Fig. 10. Dispersion curves, $\bar{k}_r = 0.01, \bar{k}_c = 0.1$: (a) $\bar{v} = 0$, Classical model; (b) $\bar{v} = 0$, High-order model; (c) $\bar{v} = 0.3$, Classical model; (d) $\bar{v} = 0.3$, High-order model; (e) $\bar{v} = 0.7$, Classical model; (f) $\bar{v} = 0.7$, High-order model.

i) The dispersion curves are symmetric with respect to the frequency axis for a stationary ring whereas this symmetry is broken when the ring rotates.
ii) For the stationary and sub-critically rotating case, waves are generated only when the excitation frequency of the load exceeds a critical value. This critical frequency occurs when the horizontal line $\bar{\Omega}_f$ is tangent to the dispersion curve. For the stationary ring case, the critical frequency is the first cut-off frequency. However, the critical frequency has a lower value than the first cut-off frequency of the corresponding stationary ring case when the ring rotates sub-critically.
iii) For the stationary and sub-critically rotating case, similar steady-state responses are expected regardless of the choice of models if the excitation frequency is not too high. Taking sub-critical speed $\bar{v} = 0.3$ as an example, if one assumes the frequency of the load to be $\bar{\Omega}_f = 0.15$, two waves are excited since

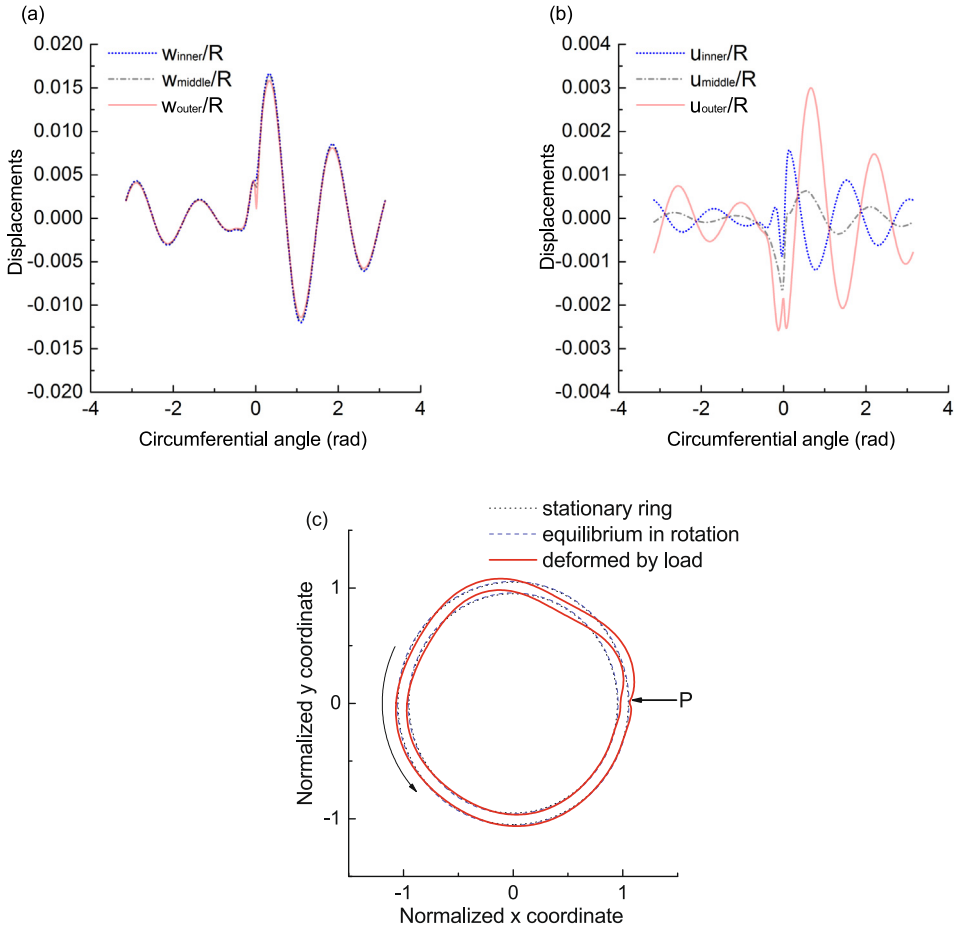

Fig. 11. High-order model, displacements under a harmonic load, $\bar{v} = 0.3, \bar{k}_r = 0.01, \bar{k}_c = 0.1, \zeta = 0.002, \bar{\Omega}_f = 0.15$: (a) Radial displacement; (b) Circumferential displacement; (c) Ring deformation. The ring deformation is scaled by 5.

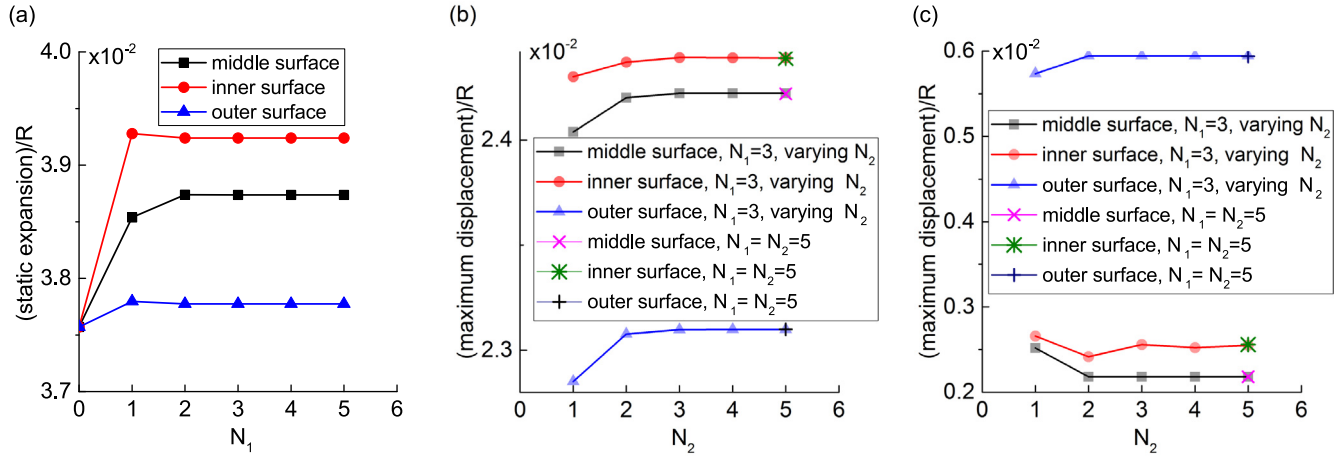

Fig. 12. Convergence check of the displacements at different positions of the ring for $\bar{v} = 0.7, \bar{k}_r = 0.01, \bar{k}_c = 0.1, \zeta = 0.002$: (a) Static radial expansion due to rotation; (b) Radial displacement; (c) Circumferential displacement.

there are two intersections between the load frequency line and the dispersion curves as shown in Fig. 10(c–d). The crossing points in Fig. 10(c) and (d) are located at similar places. Thus, the waves generated are expected to be similar. Note that the dispersion analysis is based on the undamped case, the actual displacements predicted by the classical and high-order model may differ to some extent since the same damping value may have quantitatively different effect on the actual responses according to different models. The displacements and ring deformation pattern for this case are shown in Fig. 11 using the high-order model.

iv) When the ring rotates super-critically (Fig. 10(e–f)), the intersections between the dispersion curves and the horizontal axis confirm that waves are excited by a stationary load at zero excitation frequency, namely $\bar{\Omega}_f = 0$. Unlike the stationary and sub-critically rotating case, the waves predicted by the classical and the high-order models are no longer similar for any frequency since the crossing points of the excitation frequency and the dispersion curves predicted by these models are different.

3.3. Discussion on the convergence of higher order terms for the dynamic responses

In previous sections, $N_1 = N_2 = 5$ is chosen to obtain the dynamic responses of a rotating ring subjected to a stationary ring. The convergence of the dynamic response for the choice of $N_1 = N_2 = 5$ is checked. It is not necessary to have the same number of terms for the radial and circumferential displacements. It should be mentioned that the terms needed depend on the system parameters and the type of loadings, the rotational speeds, etc. Therefore, there is no unique choice of terms for all situations. The general idea for the choice of terms is that, the more complicated distributions of stress and displacement along the thickness, the more terms are needed. One also needs to first check the convergence for the static equilibrium before examining convergence of the dynamic responses.

As an example of the convergence check, the case in Fig. 9, namely $\bar{k}_r = 0.01, \bar{k}_c = 0.1$ and $\bar{v} = 0.7$, is plotted in Fig. 12. The convergence examinations are done for the axisymmetric radial expansion due to rotation and the maximum dynamic response caused by the stationary load for different locations on the ring. The number of terms of circumferential displacement does not influence the convergence for the rotation-induced static expansion only has radial deformations. One can see that up to $N_1 = 3$ the static expansion converges. After the convergence of the static expansion is assured, the convergence of the dynamic responses is examined. As shown in Fig. 12(b–c), the choice of $N_1 = N_2 = 5$ gives convergent results for both the radial and circumferential displacements although it is not the minimum requirement.

4. Resonance: rotating ring versus moving load

Two configurations of loading situation of a ring structure are of interest in practice: (i) a stationary ring subjected to a circumferentially moving constant load and (ii) a rotating ring under a

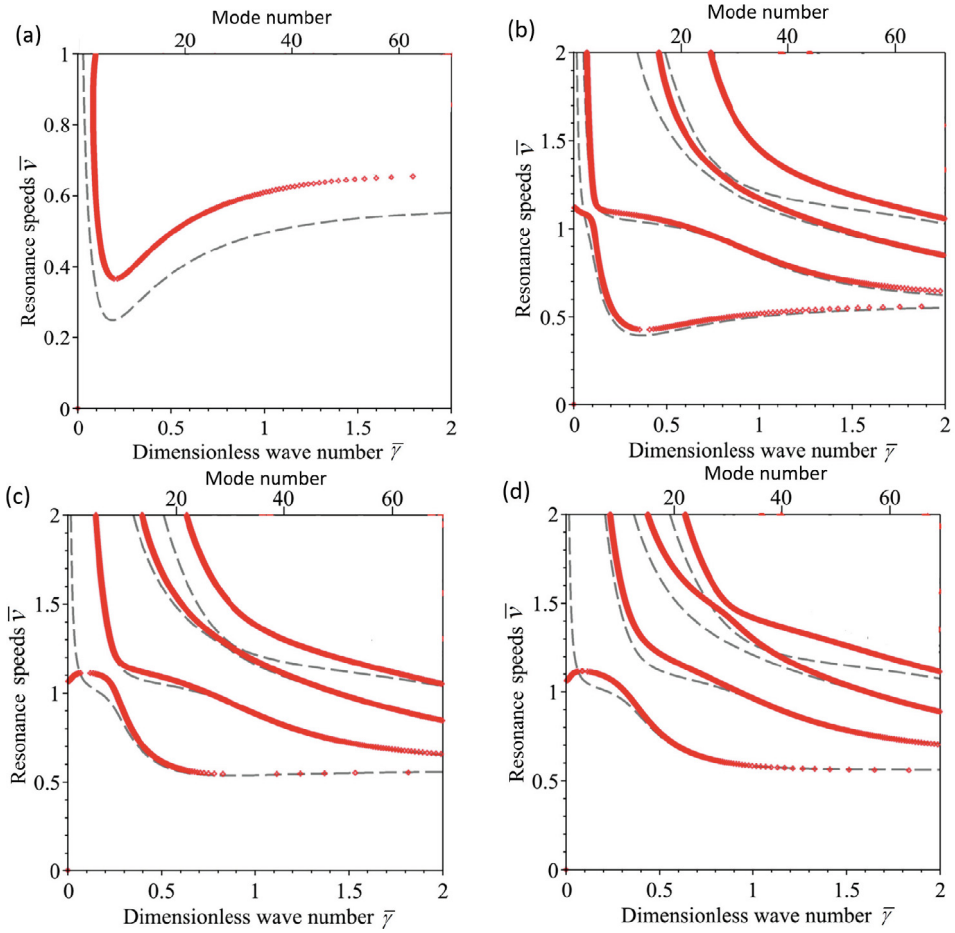

Fig. 13. Comparison of resonance speeds, $h/R = 0.1, \bar{k}_c = 0.001$ using the high-order model with increasing stiffness of radial springs. Grey dashed line for moving load case; Red dotted lines for rotating ring case: (a) $\bar{k}_r = 0.001$; (b) $\bar{k}_r = 0.01$; (c) $\bar{k}_r = 0.1$; (d) $\bar{k}_r = 0.5$. (For interpretation of the references to colour in this figure legend, the reader is referred to the web version of this article.)

stationary constant load. In this section, resonance speeds and steady-state responses for both cases are compared. The aim of this comparison is to show to what extent these two cases can be treated as equal. The corresponding high-order stationary ring model used for comparison is obtained by setting $\Omega = 0$ for the high-order rotating ring model.

4.1. Resonance speeds

The load speeds causing resonance of a stationary ring subjected to a constant point load moving circumferentially are well known (Bogy et al., 1974; Metrikine and Tochilin, 2000; Forbes and Randall, 2008; Soedel, 1975):

$$\Omega = \omega_n / n \tag{46}$$

in which n is the circumferential mode number and $n \geqslant 1$. The minimum resonance speed (the critical speed) is the lowest value of Eq. (46). Eq. (46) is rather transparent and can be interpreted straightforwardly since the periodically applied moving load expressed by Dirac function $\delta(\theta - \Omega t)$ can be represented by a Fourier series as (Leung and Pinnington, 1987)

$$\delta(\theta - \Omega t) = \frac{1}{2\pi} + \frac{1}{\pi}\sum_{n=1}^{\infty} \cos(n\theta - n\Omega t), \tag{47}$$

the loading has components with frequencies equal to $n\Omega$. Therefore one expects resonance when $\omega_n = n\Omega$, which yields Eq. (46).

Resonance speeds of a rotating ring subjected to a stationary constant load satisfy the condition $\bar{\omega}_n = 0$ in which $\bar{\omega}_n$ is the natural frequency calculated in a space-fixed reference system (Lin and Soedel, 1988; Soedel, 2004; Lu et al., 2019; Lu et al., 2017; Lu and Metrikine, 2015). By substituting $\bar{\omega} = 0$ into the frequency equation (Lu et al., 2019), one can solve for resonance speeds for each circumferential wavenumber.

It is worth mentioning that resonance occurs only for certain parameters of a rotating ring subjected to a stationary load of constant magnitude. Figs. 13 and 14 show the comparisons of resonance speeds, as functions of the mode number, between moving load and rotating ring case with different values of the foundation stiffness. The lower abscissa in each plot is the dimensionless wavenumber which is given by $\bar{\gamma} = n\sqrt{EI/(EA)}/R$ as shown in Eq. (11), whereas the upper abscissa is the corresponding discrete circumferential mode number n. All the chosen parameters represent relatively stiff foundation (soft ring) configuration since only in this case resonance speeds of rotating rings exist.

In Figs. 13(a) and 14(a) the upper limit of the plots is set at $\bar{v} = 1$ and therefore only the lowest branch of resonance speeds is shown. The reason is that at higher speeds, the predictions of other branches are not accurate since the static expansion approaches extremely high value. Generally, rotation stiffens the ring, therefore, the resonance speeds of rotating ring case are higher than those in the moving load case as shown in Figs. 13(a) and 14(a). With increasing $\bar{k}_r$, the resonance speeds for the two lower branches of both cases become close, except in

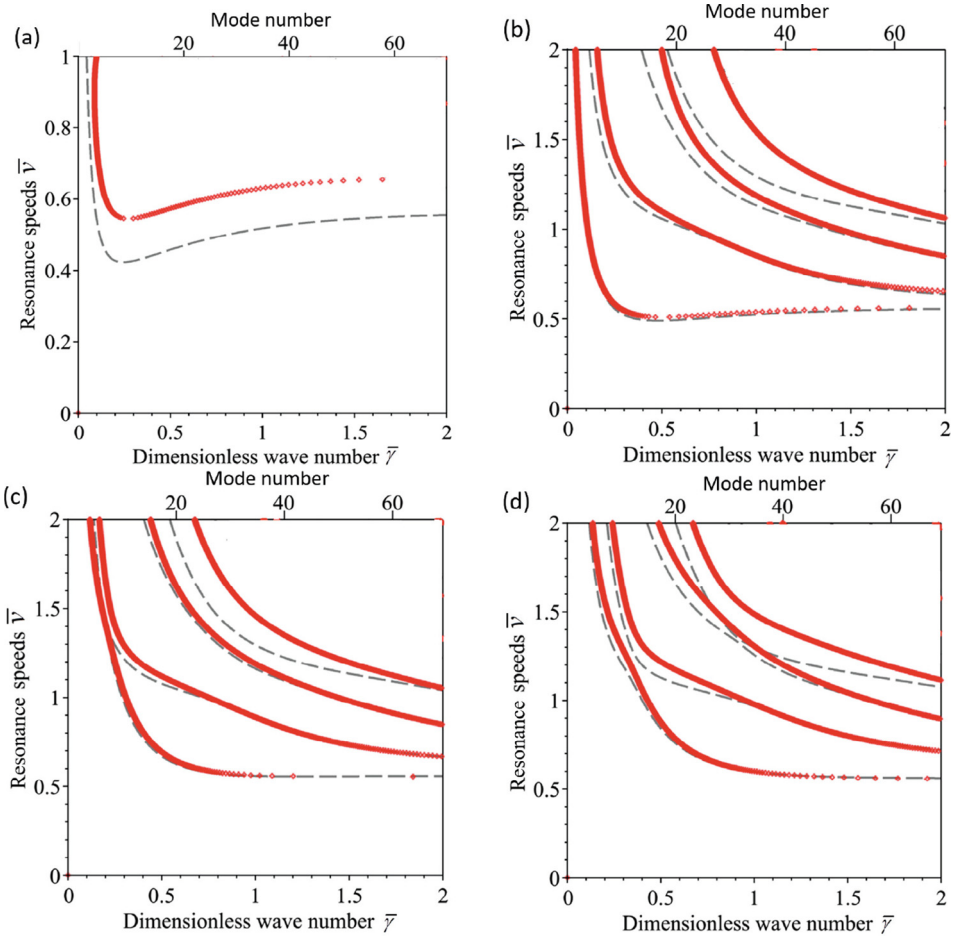

Fig. 14. Comparison of resonance speeds, $h/R = 0.1, \bar{k}_c = 0.1$ using the high-order model with increasing stiffness of radial springs. Grey dashed line for moving load case; Red dotted lines for rotating ring case: (a) $\bar{k}_r = 0.001$; (b) $\bar{k}_r = 0.01$; (c) $\bar{k}_r = 0.1$; (d) $\bar{k}_r = 0.5$. (For interpretation of the references to colour in this figure legend, the reader is referred to the web version of this article.)

the lower wavenumber ranges as shown in Figs. 13(a) and 14(a) and (b)–(d). For the two higher branches of resonance speeds, the differences are still noticeable.

The tangential stiffness $\bar{k}_c$ has a more profound influence on the resonance speeds for the lower mode (wave) numbers. For small tangential stiffness of the foundation, divergence instability of mode $n = 0$ may occur for rotating rings as shown in Fig. 13(b–d). However, for higher values of both $\bar{k}_c$ and $\bar{k}_r$, the resonance speeds of the moving load case and rotating ring case are closer even for lower mode numbers as shown in Fig. 14.

The minimum resonance speed in Figs. 13 and 14 is a critical speed at which a wave-like steady-state deformation pattern is initiated. For the parameters shown in Figs. 13(c–d) and 14(c–d), the critical speed converges to the Rayleigh wave speed with increasing wavenumber and a Rayleigh wave resonance is expected when a stationary constant load is applied (Rabier and Oden, 1989; Karttunen and von Hertzen, 2013).

4.2. The maximum deflection of the ring versus velocity

The maximum displacement at the middle surface ($D_{\max}$ is defined as $\max\left\{\sqrt{w_0^2 + u_0^2}\right\}$) of a rotating ring with the same parameters as used in Section 3.2 is shown in Fig. 15(a). Three damping coefficients are chosen. As expected, higher damping value reduces the displacement and suppresses resonance peaks that correspond to higher frequencies.

The maximum displacement of the ring using rotating ring-stationary load model is compared with that predicted using the corresponding stationary ring-moving load model in Fig. 15(b). For the chosen parameters, the resonance speeds of both cases are quite similar as shown in Fig. 14(b). However, the responses are different under the same load as shown in Fig. 15(b), especially when the relative speeds between the load and the ring exceed the minimum resonance speed. The rotation of the ring stiffens the ring, resulting in smaller responses. A similar problem, namely the dynamic response of a cylinder cover in relative motion with a load is studied in Karttunen and von Hertzen (2014). It is concluded that the effect of rotation is of no importance. However, the moving load on stationary ring and the rotating ring under stationary load cases can only be considered equivalent when the relative speeds between the ring and the load are low or the responses are mainly governed by the $n = 1$ mode. In general, these two cases need to be distinguished. Firstly, if resonance speeds exist, these can be very different in the two cases under consideration as shown in Figs. 13(a) and 14(a), which will result in different dynamic responses. Secondly, even for system parameters which result in similar critical speeds, e.g. Fig. 14(b), the responses under the same load can be different due to the rotation effects as is shown in Fig. 15(b).

5. Conclusions

The steady-state response of a rotating ring on an elastic foundation subjected to a stationary load is investigated in this paper. A high-order rotating ring model which accounts for the through-thickness variations of stresses and displacements is used in the framework of plane strain assumption. The method of the images, which gives a semi-analytical solution to the problem, is applied to obtain the dynamic response. The predicted stationary deformation pattern of a super-critically rotating ring subjected to a constant stationary load confirms the experimentally observed stationary deformation patterns in rolling tyres, not only qualitatively; also the predicted deformation patterns around the ring and the experimental observation are in agreement.

The characteristics of the response to a line(point) load with constant magnitude are highly dependent on the ring parameters and the stiffness of the foundation. The dimensionless parameter $\bar{k}_r$, defined as the ratio of the stiffness of the elastic foundation to the bending stiffness of the ring, is found to have dominant influence on the response. For a stiff ring with soft foundation (low value of $\bar{k}_r$), the response is mainly governed by the modes with low mode numbers, especially the $n = 1$ mode. Thus, for a stiff ring subjected to a stationary constant load, both the classical model and the high-order model give similar predictions of the dynamic response since higher order corrections influence mostly the ring deformation at higher modes.

For soft rings on stiff foundation (large $\bar{k}_r$) subjected to a constant stationary load, resonance speeds exist. Physically speaking, high value of $\bar{k}_r$ means that the ring is very flexible in comparison with the supporting elastic foundation. When the ring rotates at speeds lower than the minimum resonance speed (sub-critically), the deformation is localised around the loading point. Viscosity causes asymmetry of the ring deformation pattern with respect to the load. When the ring rotates super-critically, waves are generated in front of and behind the load. This is the first time such waves are predicted using a rotating ring model with rotation-induced hoop tension being properly considered. In the leading edge, waves have shorter wavelengths and higher frequencies. In the trailing edge, waves with longer wavelengths are excited. The amplitudes of those are larger than the ones in the leading edge. The high frequency waves in the leading edge are sensitive to damping in the ring and almost disappear at realistic damping values. This is exactly what is observed in experiments with rolling tyres. In the super-critically rotating case, the high-order model

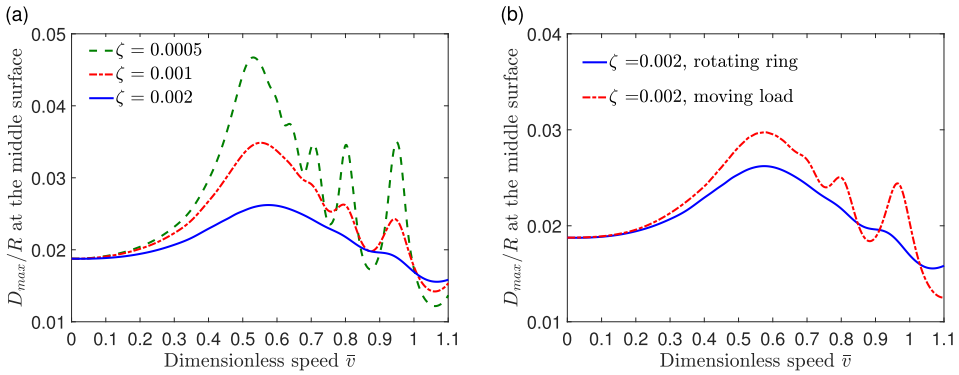

Fig. 15. Maximum deflection at the middle surface versus velocity, $\bar{k}_r = 0.01$, $\bar{k}_c = 0.1$: (a) rotating ring case with various damping values; (b) Comparison between rotating ring and moving load cases.

and the classical one give considerably different predictions of the response. When a stationary harmonic load is applied, for the stationary ring and sub-critically rotating ring case, the classical model can be used in a certain frequency range. However, waves predicted by the classical model and by the high-order model are different for all excitation frequencies in the case of a super-critically rotating ring.

The equivalence of the rotating ring under a stationary constant load case and a stationary subjected to a moving constant load case are investigated by comparing their resonance speeds, as well as the steady-state responses. This issue is rarely discussed in the literature. In the few references where two cases are studied, they are considered as equal. It is found that these two cases need to be distinguished even for system parameters which result in similar critical speeds in this work.

Declaration of Competing Interest

The authors declare that they have no known competing financial interests or personal relationships that could have appeared to influence the work reported in this paper.

Acknowledgements

The first author would like to thank the China Scholarship Council (CSC) (No. 201207090006) for the financial support to this work.

Appendix A. Energy expressions

To derive the complete equations of motion and the boundary conditions, we make use of Hamilton's principle, i.e.

$$\delta\int_{t_1}^{t_2}(S+V-T-W)\,\mathrm{d}t=\int_{t_1}^{t_2}(\delta S+\delta V-\delta T-\delta W)\,\mathrm{d}t=0 \tag{A.1}$$

where S is the strain energy, T is the kinetic energy, V is the potential energy stored in the elastic foundation and W is the energy input from external load as shown in Eq. (1).

The variation of strain energy is given by

$$\delta S=\delta S_1+\delta S_2+\delta S_3 \tag{A.2}$$

in which δS_1 is the variation of the strain energy associated with circumferential strain, δS_2 is the addition to that due to a non-zero radial strain, and δS_3 is the strain energy related to shear strain.

Integrating δS_1 between two time instants, t_1 and t_2, one obtains

$$\int_{t_1}^{t_2}\delta S_1\,\mathrm{d}t=b\int_{t_1}^{t_2}\int_{-h/2}^{h/2}\int_0^{2\pi}(\sigma_\theta\,\delta\varepsilon_\theta)r\,\mathrm{d}\theta\mathrm{d}z\mathrm{d}t. \tag{A.3}$$

The integration of δS_2 from t_1 to t_2 gives

$$\int_{t_1}^{t_2}\delta S_2\,\mathrm{d}t=b\int_{t_1}^{t_2}\int_{-h/2}^{h/2}\int_0^{2\pi}(\sigma_r\,\delta\varepsilon_r)r\,\mathrm{d}\theta\mathrm{d}z\mathrm{d}t. \tag{A.4}$$

The integration of δS_3 from t_1 to t_2 reads

$$\int_{t_1}^{t_2}\delta S_3\,\mathrm{d}t=b\int_{t_1}^{t_2}\int_{-h/2}^{h/2}\int_0^{2\pi}(\tau_{\theta r}\,\delta\gamma_{\theta r})r\,\mathrm{d}\theta\mathrm{d}z\mathrm{d}t. \tag{A.5}$$

In Eqs. (A.3)–(A.5):

$$\begin{Bmatrix}\sigma_r\\ \sigma_\theta\\ \tau_{r\theta}\end{Bmatrix}=\begin{bmatrix}2\mu+\lambda & \lambda & 0\\ \lambda & 2\mu+\lambda & 0\\ 0 & 0 & \mu\end{bmatrix}\begin{Bmatrix}\varepsilon_r\\ \varepsilon_\theta\\ \gamma_{r\theta}\end{Bmatrix} \tag{A.6}$$

and (Stein, 1986)

$$\varepsilon_\theta=\varepsilon_0+\frac{1}{2}(\beta)^2,\varepsilon_r=w_{,r}+\frac{1}{2}(u_{,r})^2,\gamma_{\theta r}=(1-w_{,r})u_{,r}-\beta\eta \tag{A.7}$$

where

$$\begin{aligned}&\varepsilon_0=\tfrac{u'}{r}+\tfrac{w}{r},\beta=\tfrac{u}{r}-\tfrac{w'}{r},\eta=1-\varepsilon_0,\\ &u_{,r}=\tfrac{\partial u}{\partial r}=\tfrac{\partial u}{\partial z},w_{,r}=\tfrac{\partial w}{\partial r}=\tfrac{\partial w}{\partial z}.\end{aligned} \tag{A.8}$$

The prime stands for the partial derivative with respect to θ whereas the subscript $(,r)$ stands for the partial derivative with respect to r.

The velocity vector of a differential element of the ring in the space-fixed frame reads

$$\dot{\mathbf{r}}\quad=(\dot{w}+(w'-u)\Omega)\mathbf{i}+(\dot{u}+(r+w+u')\Omega)\mathbf{j} \tag{A.9}$$

in which $\mathbf{i}$ and $\mathbf{j}$ are unit vectors in the radial and circumferential directions, respectively. The overdot represents partial derivative with respect to time. Integration over time of the kinetic energy variation can be evaluated as

$$\int_{t_1}^{t_2}\delta T\,\mathrm{d}t=\frac{\rho b}{2}\int_{t_1}^{t_2}\int_{-h/2}^{h/2}\int_0^{2\pi}\delta(\dot{\mathbf{r}}\cdot\dot{\mathbf{r}})r\,\mathrm{d}\theta\mathrm{d}z\mathrm{d}t. \tag{A.10}$$

The variation of the potential energy stored in the elastic foundation includes two parts, namely

$$\delta V=\delta V_1+\delta V_2 \tag{A.11}$$

in which δV_1 is related to the radial springs which connect the inner surface of the ring to its hub while δV_2 to the shear tangential springs. The integration over time of δV_1 and δV_2 yields

$$\int_{t_1}^{t_2}\delta V_1\,\mathrm{d}t=b\int_{t_1}^{t_2}\int_0^{2\pi}\left((k_r w r\,\delta w)|_{z=-h/2}\right)\mathrm{d}\theta\mathrm{d}t \tag{A.12}$$

and

$$\int_{t_1}^{t_2}\delta V_2\,\mathrm{d}t=b\int_{t_1}^{t_2}\int_0^{2\pi}\left((k_c u r\,\delta u)|_{z=-h/2}\right)\mathrm{d}\theta\mathrm{d}t. \tag{A.13}$$

Upon substitution of Eqs. (A.3)–(A.13) and (1) to (A.1) and by following basic variational calculus, one can obtain the governing Eqs. 5,6 after linearisation. For detailed derivations using the Hamilton's principle one is referred to Lu et al. (2019).

Appendix B. Expressions in Eqs. 5,6

Under the plane strain assumption, the expressions for $\mathrm{I}_1^{\mathrm{lin}},\mathrm{I}_2^{\mathrm{lin}},f_1^{\mathrm{lin}}$ through f_4^{lin} in Eqs. 5,6 are given by Lu et al. (2019):

$$\begin{aligned}
\mathrm{I}_1^{\mathrm{lin}}&=\sigma_\theta^{\mathrm{lin}}+\sigma_\theta^0(\beta)\prime-\left(r\,\sigma_r^{\mathrm{lin}}\right)_{,r}-[(\tau_{\theta r}\,\eta)\prime]^{\mathrm{lin}},\\
\mathrm{I}_2^{\mathrm{lin}}&=-(\sigma_\theta^{\mathrm{lin}})\prime+\sigma_\theta^0\,\beta-\left[r(\sigma_r^0)u_{,r}\right]_{,r}-(\tau_{\theta r}\,\eta)^{\mathrm{lin}}-\left\{[r\,\tau_{\theta r}(1-w_{,r})]_{,r}\right\}^{\mathrm{lin}}\\
f_1^{\mathrm{lin}}&=\left[r(2\mu+\lambda)\tfrac{\partial w}{\partial r}+\lambda(u\prime+w)\right]|_{z=h/2},\\
f_2^{\mathrm{lin}}&=\left[r(2\mu+\lambda)\tfrac{\partial w}{\partial r}+\lambda(u\prime+w)-k_r w r\right]|_{z=-h/2},\\
f_3^{\mathrm{lin}}&=\left\{\tfrac{G(r-w_{\mathrm{e}})(1-w_{\mathrm{e},r})}{r}(w\prime-u)+\left[Gr\left(1+(w_{\mathrm{e},rr})^2\right)\right.\right.\\
&\quad\left.\left.+\lambda\left(rw_{\mathrm{e},r}+w_{\mathrm{e}}\right)\right]u_{,r}\right\}|_{z=h/2},\\
f_4^{\mathrm{lin}}&=\left\{\frac{G(r-w_{\mathrm{e}})(1-w_{\mathrm{e},r})}{r}(w\prime-u)+\left[Gr\left(1+(w_{\mathrm{e},rr})^2\right)\right.\right.\\
&\quad\left.\left.+\lambda\left(rw_{\mathrm{e},r}+w_{\mathrm{e}}\right)\right]u_{,r}-k_c u r\right\}|_{z=-\frac{h}{2}}.
\end{aligned} \tag{B.1}$$

The expressions with superscript "lin" in Eq. (B.1) are the linearised versions of the corresponding expressions. w_{e} is the axisymmetric radial expansion caused by rotation which is given as:

$$w_e(z) = \sum_{l=0}^{l=N_1} w_{el} z^l. \tag{B.2}$$

The radial expansion $w_e(z)$ is a function of the rotational speed and is solved in Lu et al. (2019). The stresses σ_r^0 and σ_θ^0 are pre-stresses caused by rotation in radial and circumferential directions, respectively. From the Hooke's law Eq. (A.6), the prestress in radial direction is given by

$$\sigma_r^0 = 2\mu\varepsilon_r^0 + \lambda\left(\varepsilon_r{}^0 + \varepsilon_\theta^0\right) \tag{B.3}$$

and in circumferential direction it reads

$$\sigma_\theta^0 = 2\mu\varepsilon_\theta^0 + \lambda\left(\varepsilon_r{}^0 + \varepsilon_\theta^0\right) \tag{B.4}$$

where the strains caused by rotation are

$$\varepsilon_r^0 = \frac{\partial w_e}{\partial r}, \varepsilon_\theta^0 = \frac{w_e}{r}. \tag{B.5}$$

The velocities v_1 and v_2 in Eqs. 5,6 are related to the vibrational velocities, namely (Lu et al., 2019)

$$v_1 = (\dot{w} + (w' - u)\Omega), \quad v_2 = (\dot{u} + (u' + w)\Omega). \tag{B.6}$$

Appendix C. The coefficient matrix, displacement and force vectors

The coefficient matrix **C** is of the order $(N_1 + N_2 + 2) \times (N_1 + N_2 + 2)$. The displacement vector **a** and the force vector **f** are of the order $(N_1 + N_2 + 2) \times 1$.

$$\mathbf{C} = \begin{bmatrix}
\Delta_{w00} & \Delta_{w01} & \cdots & \Delta_{w0l} & \cdots & \Delta_{w0N_1} & \Delta_{u00} & \Delta_{u01} & \cdots & \Delta_{u0q} & \cdots & \Delta_{u0N_2} \\
\Delta_{w10} & \Delta_{w11} & \cdots & \Delta_{w1l} & \cdots & \Delta_{w1N_1} & \Delta_{u10} & \Delta_{u11} & \cdots & \Delta_{u1q} & \cdots & \Delta_{u1N_2} \\
\vdots & \vdots & \cdots & \vdots & \cdots & \vdots & \vdots & \vdots & \cdots & \vdots & \cdots & \vdots \\
\Delta_{wl0} & \Delta_{wl1} & \cdots & \Delta_{wll} & \cdots & \Delta_{wlN_1} & \Delta_{ul0} & \Delta_{ul1} & \cdots & \Delta_{ulq} & \cdots & \Delta_{ulN_2} \\
\cdots & \vdots & \cdots & \vdots & \cdots & \vdots & \vdots & \vdots & \cdots & \vdots & \cdots & \vdots \\
\Delta_{wN_10} & \Delta_{wN_11} & \cdots & \Delta_{wN_1l} & \cdots & \Delta_{wN_1N_1} & \Delta_{uN_10} & \Delta_{uN_11} & \cdots & \Delta_{uN_1q} & \cdots & \Delta_{uN_1N_2} \\
\Delta_{w(N_1+1)0} & \Delta_{w(N_1+1)1} & \cdots & \Delta_{w(N_1+1)l} & \cdots & \Delta_{w(N_1+1)N_1} & \Delta_{u(N_1+1)0} & \Delta_{u(N_1+1)1} & \cdots & \Delta_{u(N_1+1)q} & \cdots & \Delta_{u(N_1+1)N_2} \\
\Delta_{w(N_1+2)0} & \Delta_{w(N_1+2)1} & \cdots & \Delta_{w(N_1+2)l} & \cdots & \Delta_{w(N_1+2)N_1} & \Delta_{u(N_1+2)0} & \Delta_{u(N_1+2)1} & \cdots & \Delta_{u(N_1+2)q} & \cdots & \Delta_{u(N_1+2)N_2} \\
\vdots & \vdots & \cdots & \vdots & \cdots & \vdots & \vdots & \vdots & \cdots & \vdots & \cdots & \vdots \\
\Delta_{w(N_1+q+1)0} & \Delta_{w(N_1+q+1)1} & \cdots & \Delta_{w(N_1+q+1)l} & \cdots & \Delta_{w(N_1+q+1)N_1} & \Delta_{u(N_1+q+1)0} & \Delta_{u(N_1+q+1)1} & \cdots & \Delta_{u(N_1+q+1)q} & \cdots & \Delta_{u(N_1+q+1)N_2} \\
\vdots & \vdots & \cdots & \vdots & \cdots & \vdots & \vdots & \vdots & \cdots & \vdots & \cdots & \vdots \\
\Delta_{w(N_1+N_2+1)0} & \Delta_{w(N_1+N_2+1)1} & \cdots & \Delta_{w(N_1+N_2+1)l} & \cdots & \Delta_{w(N_1+N_2+1)N_1} & \Delta_{u(N_1+N_2+1)0} & \Delta_{u(N_1+N_2+1)1} & \cdots & \Delta_{u(N_1+N_2+1)q} & \cdots & \Delta_{u(N_1+N_2+1)N_2}
\end{bmatrix}. \tag{C.1}$$

All the entries can be obtained by any symbolic computation software. The displacement vector in frequency-wavenumber domain is given as

$$\mathbf{a} = \begin{bmatrix}
\tilde{\tilde{W}}_0^{(\bar{\omega},\bar{\gamma})} & \tilde{\tilde{W}}_1^{(\bar{\omega},\bar{\gamma})} & \cdots & \tilde{\tilde{W}}_l^{(\bar{\omega},\bar{\gamma})} & \cdots & \tilde{\tilde{W}}_{N_1}^{(\bar{\omega},\bar{\gamma})} & \tilde{\tilde{U}}_0^{(\bar{\omega},\bar{\gamma})} & \tilde{\tilde{U}}_1^{(\bar{\omega},\bar{\gamma})} \\
\cdots & \tilde{\tilde{U}}_q^{(\bar{\omega},\bar{\gamma})} & \cdots & \tilde{\tilde{U}}_{N_2}^{(\bar{\omega},\bar{\gamma})} & & & & &
\end{bmatrix}^T. \tag{C.2}$$

The force vector is given by

$$\mathbf{f} = [P_{w0} \quad P_{w1} \quad \cdots \quad P_{wl} \quad \cdots \quad P_{wN_1} \quad P_{u0} \quad P_{u1} \quad \cdots \quad P_{uq} \quad \cdots \quad P_{uN_2}]^T. \tag{C.3}$$

Since the load is only applied in the radial direction

$$P_{wl} = -2\pi\bar{P}_0\delta(\bar{\omega} - \bar{\Omega}_f), \quad (l = 0, 1, 2, 3 \ldots N_1), \tag{C.4}$$

whereas

$$P_{uq} = 0, \quad (q = 0, 1, 2, 3 \ldots N_2), \tag{C.5}$$

meaning that all the components acting in the circumferential direction are null.

References

Bogy, D., Greenberg, H., Talke, F., 1974. Steady solution for circumferentially moving loads on cylindrical shells. IBM J. Res. Dev. 18, 395–400. https://doi.org/10.1147/rd.185.0395.

Chatterjee, A., Cusumano, J.P., Zolock, J.D., 1999. On contact-induced standing waves in rotating tires: experiment and theory. J. Sound Vib. 227, 1049–1081. https://doi.org/10.1006/jsvi.1999.2395.

Cho, J., Kim, K., Jeong, H., 2007. Numerical investigation of tire standing wave using 3-D patterned tire model. J. Sound Vib. 305, 795–807. https://doi.org/10.1016/j.jsv.2007.04.049.

Cooley, C.G., Parker, R.G., 2014. Vibration of high-speed rotating rings coupled to space-fixed stiffnesses. J. Sound Vib. 333, 2631–2648. https://doi.org/10.1016/j.jsv.2014.01.005.

Endo, M., Hatamura, K., Sakata, M., Taniguchi, O., 1984. Flexural vibration of a thin rotating ring. J. Sound Vib. 92, 261–272. https://doi.org/10.1016/0022-460X(84)90560-1.

Forbes, G., Randall, R., 2008. Resonance phenomena of an elastic ring under a moving load. J. Sound Vib. 318, 991–1004. https://doi.org/10.1016/j.jsv.2008.05.021.

Gasmi, A., Joseph, P.F., Rhyne, T.B., Cron, S.M., 2012. Development of a two-dimensional model of a compliant non-pneumatic tire. Int. J. Solids Struct. 49, 1723–1740. https://doi.org/10.1016/j.ijsolstr.2012.03.007.

Gong, S., 1989. Tire ring model-literature review. Technical Report. Delft University of Technology.

Graff, K., 1975. Wave Motion in Elastic Solids. Dover Publications Inc, New York.

Graham, W., 2013. Discussion of 'On the theory of standing waves in tyres at high vehicle speeds' by V.V. Krylov and O. Gilbert, J. Sound Vib. 329 (2010) 4398–4408. J. Sound Vib. 332, 6029–6031. https://doi.org/10.1016/j.jsv.2013.06.010.

Huang, S., Soedel, W., 1987. Effects of Coriolis acceleration on the free and forced in-plane vibrations of rotating rings on elastic foundation. J. Sound Vib. 115, 253–274. https://doi.org/10.1016/0022-460X(87)90471-8.

Karttunen, A., 2015. Resonance phenomena of polymer-covered cylinders under rolling contact. Ph.D. thesis. Aalto University.

Karttunen, A.T., von Hertzen, R., 2013. A numerical study of traveling waves in a viscoelastic cylinder cover under rolling contact. Int. J. Mech. Sci. 66, 180–191. https://doi.org/10.1016/j.ijmecsci.2012.11.006.

Karttunen, A.T., von Hertzen, R., 2014. Dynamic response of a cylinder cover under a moving load. Int. J. Mech. Sci. 82, 170–178. https://doi.org/10.1016/j.ijmecsci.2014.03.026.

Karttunen, A.T., von Hertzen, R., 2016. Steady-state vibration of a viscoelastic cylinder cover subjected to moving loads. Eur. J. Mech. A/Solids 58, 202–210. https://doi.org/10.1016/j.euromechsol.2016.02.003.

Kennedy, R., Padovan, J., 1987. Finite element analysis of a steady-state rotating tire subjected to point load or ground contact. Tire Sci. Technol. 15, 243–260. https://doi.org/10.2346/1.2148792.

Krylov, V.V., 2013. Commentary on Discussion of 'On the theory of standing waves in tyres at high vehicle speeds' by V.V. Krylov and O. Gilbert, J. Sound Vib. 329 (2010) 4398–4408. J. Sound Vib. 332, 7290–7292. https://doi.org/10.1016/j.jsv.2013.08.030.

Krylov, V.V., Gilbert, O., 2010. On the theory of standing waves in tyres at high vehicle speeds. J. Sound Vib. 329, 4398–4408. https://doi.org/10.1016/j.jsv.2010.05.001.

Leung, R., Pinnington, R., 1987. Vibration of a rotating disc subjected to an in-plane force at its rim, or at its centre. J. Sound Vib. 114, 281–295. https://doi.org/10.1016/S0022-460X(87)80154-2.

Lin, J., Soedel, W., 1988. On the critical speeds of rotating thick or thin rings. Mech. Struct. Mach. 16, 439–483. https://doi.org/10.1080/08905458808960272.

Lu, T., 2019. In-plane dynamics of high-speed rotating rings on elastic foundation. Ph.D. thesis. Delft University of Technology.

Lu, T., Metrikine, A., 2015. On the existence of a critical speed of a rotating ring under a stationary point load, in: Proceedings of 43th International Summer School-Conference Advanced Problems in Mechanics (APM), SPBSPU/IPME RAS, St. Petersburg (Russia). pp. 22–27..

Lu, T., Tsouvalas, A., Metrikine, A., 2017. The in-plane free vibration of an elastically supported thin ring rotating at high speeds revisited. J. Sound Vib. 402, 203–218. https://doi.org/10.1016/j.jsv.2017.05.013.

Lu, T., Tsouvalas, A., Metrikine, A.V., 2019. A high-order model for in-plane vibrations of rotating rings on elastic foundation. J. Sound Vib. 455, 118–135. https://doi.org/10.1016/j.jsv.2019.04.037.

Macke, H., 1966. Traveling-wave vibration of gas-turbine engine shells. J. Eng. Power 88, 179–187. https://doi.org/10.1115/1.3678502.

Metrikine, A., Tochilin, M., 2000. Steady-state vibrations of an elastic ring under a moving load. J. Sound Vib. 232, 511–524. https://doi.org/10.1006/jsvi.1999.2756.

Murakami, Y., 2016. Theory of Elasticity and Stress Concentration. John Wiley & Sons.

Noga, S., Bogacz, R., Markowski, T., 2014. Vibration analysis of a wheel composed of a ring and a wheel-plate modelled as a three-parameter elastic foundation. J. Sound Vib. 333, 6706–6722. https://doi.org/10.1016/j.jsv.2014.07.019.

Padovan, J., 1975. Traveling waves vibrations and buckling of rotating anisotropic shells of revolution by finite elements. Int. J. Solids Struct. 11, 1367–1380. https://doi.org/10.1016/0020-7683(75)90064-5.

Padovan, J., 1976. On viscoelasticity and standing waves in tires. Tire Sci. Technol. 4, 233–246. https://doi.org/10.2346/1.2167224.

Potts, G., Bell, C., Charek, L., Roy, T., 1977. Tire vibrations. Tire Sci. Technol. 5, 202–225. https://doi.org/10.2346/1.2167240.

Rabier, P.J., Oden, J.T., 1989. Bifurcation in Rotating Bodies, vol. 11. Springer Verlag.

Soedel, W., 1975. On the dynamic response of rolling tires according to thin shell approximations. J. Sound Vib. 41, 233–246. https://doi.org/10.1016/S0022-460X(75)80099-X.

Soedel, W., 2004. Vibrations of Shells and Plates. CRC Press.

Stein, M., 1986. Nonlinear theory for plates and shells including the effects of transverse shearing. AIAA J. 24, 1537–1544.

Yoon, S., Park, U., Rhim, J., Yang, S.S., 2015. Tactical grade MEMS vibrating ring gyroscope with high shock reliability. Microelectron. Eng. 142, 22–29. https://doi.org/10.1016/j.mee.2015.07.004.